
A NONPARAMETRIC BAYESIAN LOCAL-GLOBAL MODEL FOR ENHANCED ADVERSE EVENT SIGNAL DETECTION IN SPONTANEOUS REPORTING SYSTEM DATA

Xin-Wei Huang

Department of Biostatistics

University at Buffalo

xinweihuangstat@gmail.com

Saptarshi Chakraborty

Department of Biostatistics

University at Buffalo

chakrab2@buffalo.edu

April 16, 2025

ABSTRACT

Spontaneous reporting system databases are key resources for post-marketing surveillance, providing real-world evidence (RWE) on the adverse events (AEs) of regulated drugs or other medical products. Various statistical methods have been proposed for AE signal detection in these databases, flagging drug-specific AEs with disproportionately high observed counts compared to expected counts under independence. However, signal detection remains challenging for rare AEs or newer drugs, which receive small observed and expected counts and thus suffer from reduced statistical power. Principled information sharing on signal strengths across drugs/AEs is crucial in such cases to enhance signal detection. However, existing methods typically ignore complex between-drug associations on AE signal strengths, limiting their ability to detect signals. We propose novel local-global mixture Dirichlet process (DP) prior-based nonparametric Bayesian models to capture these associations, enabling principled information sharing between drugs while balancing flexibility and shrinkage for each drug, thereby enhancing statistical power. We develop efficient Markov chain Monte Carlo algorithms for implementation and employ a false discovery rate (FDR)-controlled, false negative rate (FNR)-optimized hypothesis testing framework for AE signal detection. Extensive simulations demonstrate our methods' superior sensitivity—often surpassing existing approaches by a twofold or greater margin—while strictly controlling the FDR. An application to FDA FAERS data on statin drugs further highlights our methods' effectiveness in real-world AE signal detection. Software implementing our methods is provided as supplementary material.

1 Introduction

Adverse events (AEs) related to drugs and other medical products have a profound impact on public health and have received heightened attention over the past decades. While clinical trials remain the gold standard for assessing medical product safety before approval, they have limitations due to factors such as small sample sizes, ethical considerations, restricted timelines, etc., and the critical need for postmarket monitoring is increasingly recognized. For example, severe AEs such as congenital malformations from Thalidomide and liver injury from the Ketoconazole (Lavertu et al., 2021) were identified only after these drugs were approved for the U.S. market. To complement clinical trial findings with real-world evidence (RWE), continuous post-marketing surveillance—a cornerstone of contemporary pharmacovigilance—has proven essential. Accordingly, several Spontaneous Reporting System (SRS) databases have been established globally, including VigiBase (World Health Organization), and FAERS and VAERS (U.S. Food and Drug Administration). These databases collect and manage AE data for regulated medical products, such as drugs, medical devices, vaccines, and therapeutic biologics. For exposition, we focus only on drugs hereinafter, though analogous considerations apply to other medical products monitored in SRS databases.

The SRS databases serve as key resources for assessing real-world evidence in postmarket drug safety by cataloging a large number of case safety reports linking drugs to relevant AEs. For example, the FAERS database has compiled over 29 million reports by 2024. These databases are inherently observational and suffer from selection bias, measurement error, confounding, and missing data, among other factors (Markatou and Ball, 2014), precluding causal inference. Instead, the focus is on detecting *signals*: identifying drug-AE pairs that appear disproportionately more often than their *null expected* counts, derived under the assumption of independence between the drug and the AE using their marginal totals and the dataset’s grand total counts. Association analyses then estimate and assess the significance of *signal strengths*, quantifying the differences between the observed and (null) expected counts or related quantities defined by parameters of some underlying statistical model.

Numerous SRS data mining and signal detection approaches have been developed over the past decades. Examples include the proportional reporting ratio (PRR) (Evans et al., 2001), the reporting odds ratio (ROR) (Rothman et al., 2004), formal frequentist methods such as the likelihood ratio test (LRT) and its variants (Huang et al. 2011; Chakraborty et al. 2022; Ding et al. 2020; and the references cited therein), and Bayesian methods such as the Gamma Poisson Shrinker (GPS) (DuMouchel, 1999), Bayesian confidence propagation neural network (BCPNN) (Bate et al., 1998), and Dirichlet process (DP) Poisson Gamma mixture model (Hu et al., 2015). Some approaches—e.g., PRR and ROR—employ ad-hoc thresholds on empirical signal strength estimates, while the more formal methods—e.g., LRT and Bayesian approaches—employ rigorous probabilistic tools for statistically guaranteed signal detection, including controlled type I errors and false discovery rates (FDR). Despite these advances, signal detection for rare AEs and newer drugs remains challenging due to their small (marginal total) sample sizes, which leads to small observed and expected report counts in individual drugs, reducing the statistical power to detect the underlying signals. Yet, a large and growing body of research has documented the critical need for reliable pharmacovigilance signal detection precisely under these setups (see, e.g., Poluzzi et al. 2012; Sardella and Belcher 2018; Raschi et al. 2021, and the references cited therein).

Bayesian methods facilitate principled inference and signal detection for SRS data by modeling drug-AE signal strengths as model parameters with suitable priors and utilizing their posterior distributions. However, prior selec-

tion is crucial. An overly restrictive prior—e.g., a single gamma shrinkage prior for all drug-AE signal strength parameters—may cause excessive shrinkage, pulling estimates toward a single common value (Hu et al., 2015). Conversely, an overly flexible prior—e.g., independent flat priors for all parameters—may inadequately regularize their estimation, resulting in overfitting and noisy estimates. State-of-the-art Bayesian data mining approaches balance flexibility and regularization using semi/nonparametric shrinkage priors—e.g., a two-component gamma mixture prior (the GPS model of DuMouchel (1999)) or a DP mixture prior with a base gamma distribution (Hu et al., 2015)—for AE signal strengths *separately for each drug*. This stabilizes signal detection, *provided the drugs are treated either all independently or as a single group*.

However, real-world SRS databases record drugs with nuanced similarities in their AEs. For instance, various statin drugs, used to lower blood cholesterol and cardiovascular risk, share chemical compositions and function, leading to common AEs like rhabdomyolysis (Montastruc, 2023). On the other hand, small differences in drug composition and function can cause distinct AEs or variations in AE severity; e.g., myoglobinuria is typically associated with Atorvastatin but not Lovastatin (Seneff, 2016). Figure 1 shows the pairwise Spearman correlation coefficients for occurrences of 46 common AEs of six statin drugs as cataloged in FAERS (Q3 2014-Q4 2024). These correlations reveal strong yet nuanced between-drug associations: they are consistently above 0.70, ruling out independence, yet many are noticeably below one, suggesting against a single grouping of all drugs.

Existing SRS data mining approaches, both Bayesian and frequentist, rarely account for nuanced between-drug associations. Instead, they often assume either independence of drugs (the original LRT, BCPNN, GPS, and DP Poisson-Gamma) or a single group for all drugs (extended LRT of Huang et al. (2011)). These restrictive assumptions limit the statistical power and *sensitivity* for detecting signals, particularly for rare AEs and newer drugs with small observed and expected counts. Indeed, our extensive simulations (Section 4) show that existing methods suffer from poor sensitivity (after controlling FDR) when detecting signals from datasets containing multiple but weak *true* signals, rare AEs, and newer drugs.

We address this critical gap with a novel *local-global mixture DP*-based Bayesian method that balances flexibility and shrinkage in AE signal strengths for each drug while *enabling data-adaptive information sharing across drugs based on their associations*, enhancing statistical power for signal discovery. In this framework, a local DP models distinct AE signal strength patterns specific to each drug while a global process defines a common pattern across drugs; the final AE signal strengths for a drug are obtained from a probabilistic mixture of these local and global processes. By appropriately controlling the local-global contributions, our approach can flexibly capture complex between-drug associations in SRS data.

For full Bayesian inference from our model, we employ weakly informative priors customized for SRS data mining on various DP hyperparameters. This eliminates the need for any additional tuning and acknowledges all modeling uncertainty, including hyperparameters. Subsequently, we develop efficient Markov chain Monte Carlo (MCMC) algorithms for posterior computation. Signal detection is performed using a rigorous hypothesis testing framework that controls the false discovery rate (FDR) while minimizing the false negative rate (FNR), both estimated via MCMC-computed posterior probabilities. Our default implementation supports a wide range of data-generating settings for robust signal detection. Additional inferential goals, such as identifying structural zero (physically or biologically

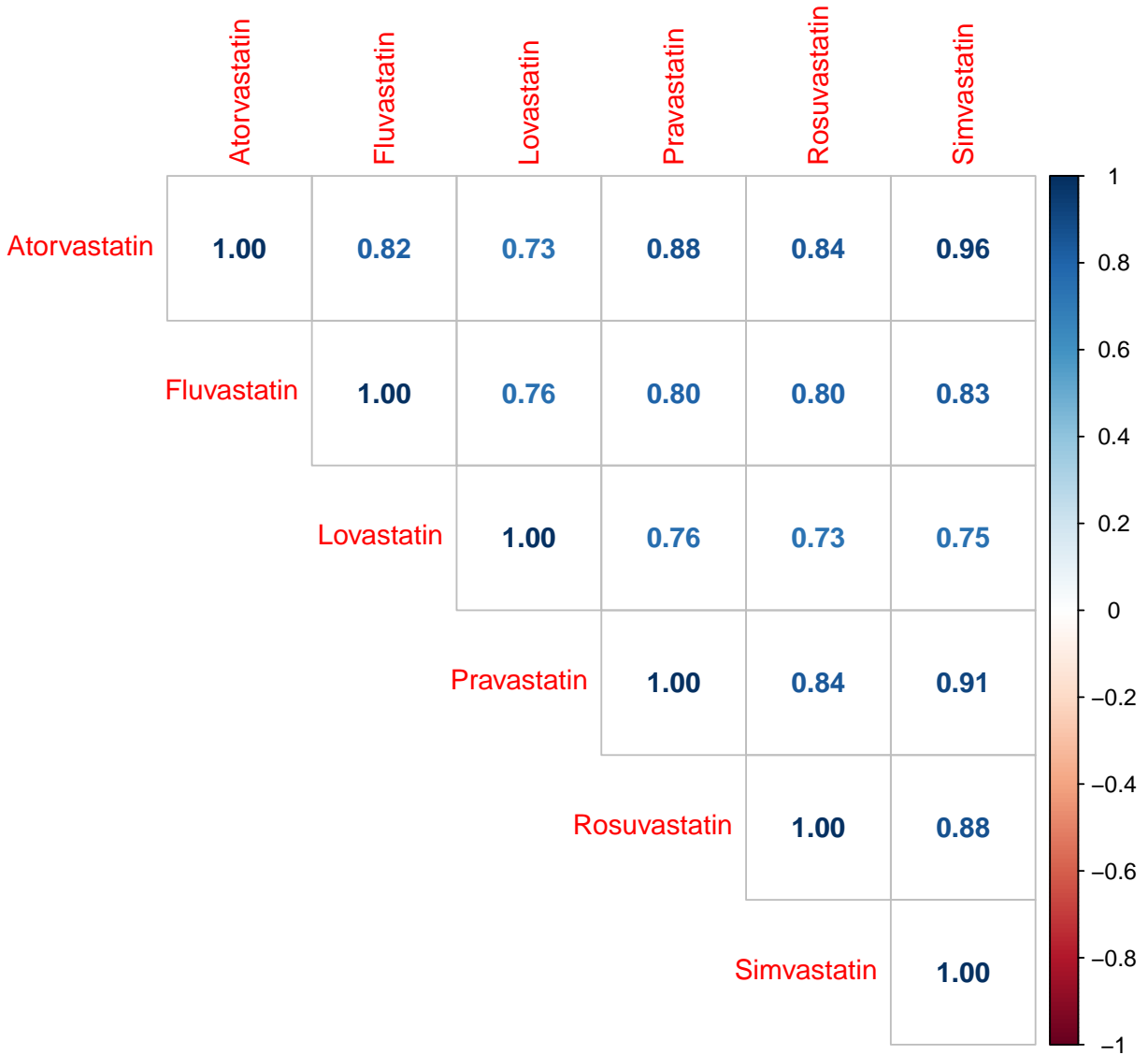


Figure 1: Spearman correlation matrix for occurrence counts of 46 common AEs (PTs) among statin drugs in the FDA FAERS data (2014 Q1-2020 Q4)

impossible drug-AE pairs), can be seamlessly incorporated through additional model layers without compromising signal detection accuracy, which we also discuss.

Our key contributions are as follows. First, we propose local-global mixture DP models for SRS signal detection (Section 3). Local-global priors are widely used in contemporary statistics (Bhadra et al. 2019 and references cited therein) and have been employed in DP modeling of grouped data, notably via hierarchical DP models (Teh et al., 2004). Our framework instead adopts a more transparent two-component mixture of DPs (Antoniak, 1974) for local-global pattern decomposition. To our knowledge, the use of local-global DP models for principled SRS data mining is novel. We develop efficient MCMC algorithms for model implementation (Section 3.3 and Supplement S.3; software in the Supplement) and leverage FDR-controlled, FNR-optimized hypothesis tests for signal detection (Section 3.4). Second, we provide an intuitive overview of DP-based SRS data mining models to aid broader understanding (Section 3.1). Third, through extensive simulations (Section 4), we show that our methods achieve comparable or superior sensitivity to existing approaches (reviewed in Supplement S.1) when only a few strong signals are present across common AEs but yield substantial sensitivity gains—often twofold or more—when many weak signals exist among rare AEs and newer drugs, all while maintaining strong FDR and type I error control. Finally, our analysis of a real-world statin dataset (Section 5) from the FDA FAERS database demonstrates our methods’ ability to effectively detect AE signals in practice.

2 SRS DATA, OUR NOTATION, AND PROBABILITY MODELS

An SRS database stores a large number of individual case safety reports that can be summarized as a high-dimensional contingency table cataloging the occurrences of multiple AEs across the rows and various drugs across the columns. Let I and J denote the total number of AEs and drugs under consideration, respectively. Further, let n_{ij} be the total number/count of reported cases for drug- j and AE- i ; $i = 1, \dots, I$ and $j = 1, \dots, J$ constituting the contingency table $((n_{ij}))$. Define $n_{i\bullet} = \sum_{j=1}^J n_{ij}$, $n_{\bullet j} = \sum_{i=1}^I n_{ij}$, and $n_{\bullet\bullet} = \sum_{i=1}^I \sum_{j=1}^J n_{ij}$.

Signal detection in SRS contingency tables often relies on the observed relative reporting rates, n_{ij}/E_{ij} , or a related quantity, as a measure of *signal strength*. Here, $E_{ij} = n_{i\bullet}n_{\bullet j}/n_{\bullet\bullet}$ represents the *null* expected count of drug- j and AE- i , assuming independence between the drug and AE. Intuitively, if $n_{ij}/E_{ij} \gg 1$, the observed frequency for (i, j) is much higher than the null expected count, suggesting a potential signal. Challenges arise for small $n_{\bullet j}$ (e.g., a new drug) and/or small $n_{i\bullet}$ (rare AE), leading to a small E_{ij} and rendering n_{ij}/E_{ij} to be noisy. Bayesian approaches parameterizing n_{ij}/E_{ij} (or an analogous quantity) using a probability model for n_{ij} can stabilize inference on signal strengths under these setups by incorporating suitable prior distributions that can facilitate principled information sharing across AEs and drugs, leading to improved signal detection.

The Poisson model $n_{ij} \sim \text{Poisson}(\lambda_{ij}E_{ij})$ is commonly used for its analytical simplicity and computational tractability. Here the *signal strength parameter* λ_{ij} parametrizes n_{ij}/E_{ij} , with the pair (i, j) considered a signal if $\lambda_{ij} \gg 1$ and non-signal otherwise. When the Poisson assumption is violated, particularly due to an excess of zero counts arising from structural zeros—i.e., drug-AE pairs that are physically or biologically impossible to co-occur—a zero-inflated Poisson (ZIP) model is often preferred. In this framework, n_{ij} is modeled as a mixture of two components: a $\text{Poisson}(\lambda_{ij}E_{ij})$ component for drug-AE pairs that can co-occur and a point mass at 0, denoted by $\delta_{\{0\}}$ (the Kronecker

delta), for structural zeros. Importantly, the structural zero positions are typically unknown and inferred from the SRS dataset.

A Bayesian SRS data mining approach begins with such a probability model for n_{ij} (e.g., Poisson or ZIP), yielding a likelihood for the signal strengths λ_{ij} that is combined with a prior distribution to derive the posterior distribution of λ_{ij} for inference. The marginal distribution of n_{ij} , after integrating over the prior, can be more flexible than the likelihood model for n_{ij} . Indeed, with an appropriate nonparametric mixture prior, a flexible marginal distribution accommodating ZIP-like behavior can be achieved using only a Poisson likelihood for n_{ij} (see Remark 3.1 under Section 3). Thus, Bayesian SRS data mining methods are less sensitive to the likelihood choice (Poisson or ZIP) when a flexible prior is used. However, if the zero-inflation probability parameters are of interest, the ZIP model remains useful.

3 NOVEL LOCAL-GLOBAL DP MODELS FOR SRS DATA MINING

We begin in Section 3.1 with a review of the drug-specific DP Poisson model of Hu et al. (2015), outlining its mechanism and providing guidance on the hyperparameters. We then introduce our novel local-global DP framework (Section 3.2) that accommodates between-drug associations and enables effective information sharing across drugs.

3.1 A conceptual overview on the DP Poisson model

Consider the Poisson likelihood $n_{ij} \sim \text{Poisson}(\lambda_{ij} E_{ij})$, with the DP prior (Hu et al., 2015):

$$\lambda_{ij} \sim D_j \equiv \sum_{h=1}^{\infty} \eta_{hj} \delta_{\{\theta_{hj}\}}; D_j \sim \text{DP}(\alpha_j, G(\beta_j)) \quad (1)$$

for the signal strength parameters $\{\lambda_{1j} \dots, \lambda_{Ij}\}$ associated with each drug j . Here $\delta_{\{\theta\}}$ denotes a degenerate distribution at θ and $\text{DP}(\alpha, G(\beta))$ is a Dirichlet process with concentration hyperparameter $\alpha > 0$ and base distribution $G(\beta) \equiv \text{Gamma}(\text{shape} = \beta, \text{rate} = \beta)$ with hyperparameter $\beta > 0$. The discrete mixture structure ensures that D_j , the prior for λ_{ij} , is almost surely discrete/categorical placing probability weights η_{hj} ; $0 \leq \eta_{hj} \leq 1$; $\sum_{h=1}^{\infty} \eta_{hj} = 1$ on atoms θ_{hj} . This permits *clustering*, allowing multiple λ_{ij} to share an atom θ_{hj} as a common value. The probability weights η_{hj} are generated using stick-breaking (Sethuraman, 1994):

$$\eta_{1j} = v_{1j}, \eta_{hj} = v_{hj} \prod_{t=1}^{h-1} (1 - v_{tj}) \text{ for } h \geq 2; v_{hj} \sim \text{independent Beta}(1, \alpha_j) \text{ for } h \geq 1 \quad (2)$$

based on the DP concentration hyperparameter $\alpha_j > 0$. Meanwhile, the atoms are generated independently from the DP base distribution: $\theta_{hj} \sim G(\beta_j)$. In practice, the infinite mixture defining D_j can be well-approximated by a finite mixture $\sum_{h=1}^K \eta_{hj} \delta_{\{\theta_{hj}\}}$ with a sufficiently large K (Ishwaran and Zarepour, 2002). This approximation simplifies model fitting and offers intuitive insights on the hyperparameters α_j and β_j , guiding their specification.

Role of α_j . The stick-breaking representation (2) elucidates that when $\alpha_j < 1$, each v_{hj} is, *on average*, greater than 1/2 with smaller α_j favoring v_{hj} closer to one. Consequently, η_{hj} decreases sharply in h , leading the mixture (1), or its finite approximation with K components, to retain only a few *non-empty* components with sufficiently large weights η_{hj} . Under a finite mixture approximation with $K_+ < K$ non-empty components, (1) models λ_{ij} using a categorical distribution with K_+ categories, placing point masses at the atoms $\theta_{1j}, \dots, \theta_{K_+j}$ with weights $\eta_{1j}, \dots, \eta_{K_+j}$. This

fosters *clustering*, restricting $\lambda_{1j}, \dots, \lambda_{Ij}$ to at most K_+ distinct values. When $K_+ < I$, multiple λ_{ij} share the same cluster h admitting the common value θ_{hj} , facilitating their pooling for information sharing. While a smaller α encourages a smaller K_+ aiding greater information sharing, a larger $K_+ (> 2)$ is permitted in the posterior when supported by data. This contrasts with the GPS framework of DuMouchel (1999) commonly used for SRS signal detection (see Section S.1 for a review) which strictly categorizes λ_{ij} into two groups, intuitively, *signal* ($\lambda_{ij} \leq 1$) and *non-signal* ($\lambda_{ij} \gg 1$). The DP framework, by allowing $K_+ > 2$, enhances heterogeneity acknowledgment within both signal and non-signal groups. Figure 2a illustrates this with $I = 6$ AEs and $K_+ = 3$ clusters.

Because a smaller α_j promotes greater information sharing, a prior assigning sufficient mass to small positive values is recommended for stable estimation of λ_{ij} . Hu et al. (2015) used a Uniform(0.2, 10) prior for α_j . We suggest a more aggressive weakly informative default prior, viz., Exponential(rate = ψ_α) with a moderately large ψ_α , e.g., $\psi_\alpha = 3$ (placing $\approx 95\%$ mass in $(0, 1)$), which favors small α_j while allowing larger values if needed. This choice also ensures conjugacy for efficient Gibbs sampling updates for MCMC implementation.

Role of β_j . The parameter β_j controls variability among the atoms θ_{hj} drawn from the base $G(\beta_j) \equiv \text{Gamma}(\text{shape} = \beta_j, \text{rate} = \beta_j)$ distribution, thereby controlling the shrinkage in λ_{ij} . Since $G(\beta_j)$ has unit mean and variance $1/\beta_j$, larger (smaller) values of β_j encourage all θ_{hj} to concentrate more (less) around 1, inducing more (less) shrinkage in λ_{ij} (around 1).

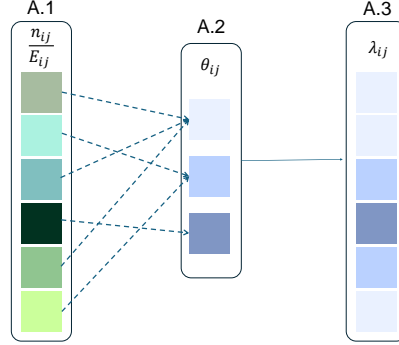
To balance shrinkage (induced by large β_j) with flexibility (small β_j), a prior that assigns sufficient mass to both small (< 1) and large (> 1) values of β_j is preferred. Hu et al. (2015) used a Uniform(0,1) prior. We suggest a *half-Cauchy* prior, $\beta_j \sim \text{Cauchy}^+(0, \psi_\beta)$, with a scale $\psi_\beta = 1/2$ ensuring equal prior probabilities for $[\beta_j < 1]$ and $[\beta_j \geq 1]$. The half-Cauchy prior has been recommended in the literature as a weakly informative default prior for scale parameters in Bayesian hierarchical models (Polson and Scott, 2012). (Note that $\beta_j \sim \text{Cauchy}^+(0, \psi_\beta)$ implies $\text{var}(\theta_{hj}) = 1/\beta_j \sim \text{Cauchy}^+(0, 1/\psi_\beta)$.)

Remark. *Zero inflation is naturally handled in the DP Poisson model through a small atom $\theta_{hj} \approx 0$, causing λ_{ij} and hence $\text{Poisson}(\lambda_{ij}E_{ij})$ to concentrate near zero for all AEs i in cluster h , effectively mimicking a degenerate-at-zero $\delta_{\{0\}}$ distribution. This yields a model virtually identical to $n_{ij} \sim \text{ZIP}(\lambda_{ij}E_{ij}, \omega_j)$, ω_j being the structural zero probability, with an analogous DP prior on λ_{ij} , producing similar posterior for λ_{ij} . Consequently, signal detection and inference on λ_{ij} remain essentially identical in both models (Section 4 provides numerical validation). However, for direct inference on the structural zero positions, the Poisson approximation of $\delta_{\{0\}}$ is insufficient, and a ZIP model $n_{ij} \sim \text{ZIP}(\lambda_{ij}E_{ij}, \omega_j)$ is needed. The same prior (3) may still be used on λ_{ij} assuming $\lambda_{ij} = 0$ if the underlying cell-specific zero-inflation indicator, say y_{ij} , indicates a structural zero to ensure identifiability. For any drug- j , the posterior distributions of y_{ij} and/or the column-specific zero-inflation probability ω_j provide inference on whether AE- i and/or any AE is a structural zero, respectively.*

3.2 The local-global DP Poisson model

The DP model in Section 3.1 enables flexible and effective signal detection for each drug separately but does not account for associations between drugs in their signal strengths. To capture these associations, we introduce the concept of local and global (prior) distributions for AE signal strengths. Specifically, we assume that the realized AE

A: DP clustering



B: Local-global structure

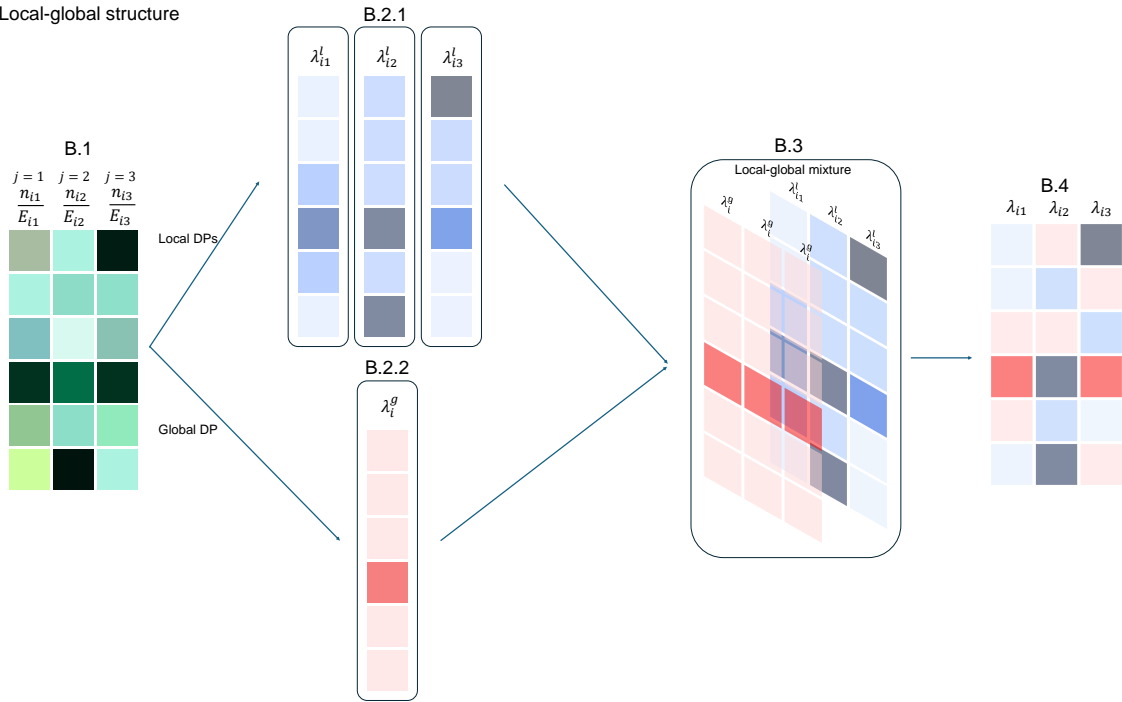


Figure 2: Schematic diagrams visualizing the mechanisms of a “local only” DP prior with one drug (**Panel A**) and local-global mixture DP prior with $J = 3$ drugs (**panel B**). Throughout, darker shades represent larger values. **Panel A:** The observed relative reporting rates n_{ij}/E_{ij} for $I = 6$ AEs for the drug j (Panel A.1) show high variability across i (different shades of green) due to randomness in observed data. The atoms $\theta_{h,j}$ (Panel A.2) of the DP prior enable clustering of $I = 6$ AE signal strengths into $K_+ = 3$ non-empty DP clusters. This ensures information sharing: the AEs ($i = 1, i = 3, i = 5$) in cluster 1 and separately the AEs ($i = 2, i = 6$) in cluster 2 (cluster memberships are visualized via arrows between Panels A.1 and A.2) share their observed (n_{ij}, E_{ij}) information to inform their cluster-specific DP atoms (single atom per cluster). These DP atoms, together with the cluster memberships, produce the final $I = 6$ AE signal strengths λ_{ij} (Panel A.3). **Panel B:** The noisy observed data (n_{ij}, E_{ij}) leading to noisy observed relative reporting rates n_{ij}/E_{ij} (Panel B.1; different shades of green) are used to produce “local” signal strengths λ_{ij}^l for $I = 6$ AEs and $J = 3$ drugs using a separate, independent local DP prior for each drug (Panel B.2.1), and global AE signal strengths λ_i^g for shared by all $J = 3$ drugs based on a common global DP prior (Column B.2.2). Probabilistic two-component mixtures of λ_{ij}^l and λ_i^g (Panel B.3) based on the local distribution indicators z_{ij}^l produce the final realized signal strengths λ_{ij} (Panel B.4).

signal strengths $\{\lambda_{1j}, \dots, \lambda_{Ij}\}$ for each drug j is drawn from a mixture of a “local” distribution specific to the drug and a “global” distribution shared among drugs with similar compositions or functions.

Under the same likelihood $n_{ij} \sim \text{Poisson}(\lambda_{ij}E_{ij})$, we consider the following local-global mixture of DP prior for λ_{ij} :

$$\begin{aligned} \lambda_{ij} &= z_{ij}^l \lambda_{ij}^l + (1 - z_{ij}^l) \lambda_i^g; \lambda_{ij}^l \sim D_j; \lambda_i^g \sim D; z_{ij}^l \sim \text{Bernoulli}(\pi^l) \\ D_j &\sim \text{DP}(\alpha_j, G(\beta_j)); D \sim \text{DP}(\alpha, G(\beta)). \end{aligned} \quad (3)$$

Here, the realized signal strengths $\{\lambda_{1j}, \dots, \lambda_{Ij}\}$ for a drug j is generated by combining local strengths $\{\lambda_{1j}^l, \dots, \lambda_{Ij}^l\}$ drawn from a drug- j -specific local distribution $D_j \sim \text{DP}(\alpha_j, G(\beta_j))$ as in (1) and global strengths $\{\lambda_1^g, \dots, \lambda_I^g\}$ generated from a global distribution $D \sim \text{DP}(\alpha, G(\beta))$ shared by all drugs. The binary *local distribution indicators* z_{ij}^l governed by the *common local proportion* π^l , determine the probabilistic mixing of λ_{ij}^l and λ_i^g .

We note that the proposed local-global mixture DP prior (3) enables information sharing in signal strengths across both AEs and drugs. Specifically, for each drug j , the realized signal strengths $\{\lambda_{i'j} : \text{all } i' \text{ with } z_{i'j} = 1\}$ exhibit the same D_j -induced clustering (see Section 3.1) as the local strengths $\{\lambda_{1j}^l, \dots, \lambda_{Ij}^l\}$, facilitating information sharing across AEs. Meanwhile, for any AE i , the signal strengths $\{\lambda_{ij'} : \text{all } j' \text{ with } z_{ij'} = 0\}$ form a cluster attaining the common global value λ_i^g , and enable information sharing across drugs (the global values $\{\lambda_1^g, \dots, \lambda_I^g\}$ themselves admitting clustering via D). Figure 2B illustrates this mechanism using $I = 6$ AEs and $J = 3$ drugs. This bi-level clustering contrasts with the single-level (AE-only) clustering induced by the DP prior of Hu et al. (2015). As demonstrated in extensive simulations (Section 4), the bi-level clustering and information sharing play a critical role in stabilizing the posterior and enhancing signal detection for λ_{ij} , particularly for drug-AE pairs where $n_{i\bullet}$ is small (rare AEs) and/or $n_{\bullet j}$ is small (newer drugs), leading to small E_{ij} .

The drugs under consideration should be similar in composition or function to justify a single global distribution D . If distinct drug groups exist with no similarities, separate global processes can be used to enable separate within-group information sharing. Additionally, SRS data often include a collapsed, heterogeneous comparator category J (e.g., “Other drugs”), serving as a baseline group with few, if any, distinct AE signals. In such cases, shrinking all λ_{iJ} toward 1 using a prior such as $\text{Gamma}(\text{shape} = \tau, \text{rate} = \tau)$ with an appropriate hyperparameter τ can improve signal detection and inference (see Supplement S.2.1).

As noted in Remark 3.1, a separate ZIP likelihood $n_{ij} \sim \text{ZIP}(\lambda_{ij}E_{ij}, \omega_j)$ is unnecessary for signal detection due to the flexibility of the DP prior. However, it may be used if direct inference on structural zero positions/probabilities is required. Complete hierarchical Bayesian representations of our Poisson and ZIP-based models are provided in Supplement S.2.1.

Remark. *The Hu et al. (2015) model can be viewed as a “local-only” special case of our local-global model, with only drug-specific local distributions D_j for λ_{ij} and no global distribution (i.e., $\pi^l = 1$). At the other extreme, a “global-only” model ($\pi^l = 0$) yields common λ_i across drugs. This is a restrictive model that cannot differentiate between drugs and only permits “global” signal detection—assessing whether an AE- i is a signal for any drug under consideration (see Supplement S.2.2 for further discussion on this model).*

Remark. *Extensive literature exists on local-global DP models for sharing information across groups while preserving DP-based clustering within each group. A common approach employs hierarchical DPs (Teh et al., 2004), where local DPs share a global DP as a base distribution. In contrast, our approach leverages a two-component DP mixture*

framework (Antoniak, 1974), separately modeling local and global AE signal strengths and thus offering a more transparent bi-level clustering over AEs and drugs, enabling more flexible estimation of the local and global parameters for greater flexibility in SRS applications.

Remark. In this paper, we focus on drug-based pharmacovigilance, identifying AE (row) signals given one or more drugs (columns in SRS contingency tables). An alternative AE-based approach discovers drugs strongly associated with a given set of AEs (Ding et al., 2020; Liu et al., 2024). A row-based version of our column-based prior (3), obtained by switching the roles of i and j , can be used for such analyses.

3.3 Full Bayesian implementation using MCMC

For full Bayesian inference on our models, we place independent weakly informative proper priors on all model hyperparameters. Along with the exponential prior for α_j and α , and half-Cauchy prior for β_j and β as suggested in Section 3.1, we consider a similar Cauchy⁺(0, ψ_τ) prior for τ with $\psi_\tau = 1/2$, and independent Uniform(0, 1) priors for the probability weight parameters, viz., π_l and ω_j (if included in the model).

We develop efficient MCMC algorithms for rigorous posterior sampling, approximating the DPs using finite mixtures with $K = O(\log(IJ))$ components. Each MCMC iteration involves data augmentation to generate latent DP mixture allocations, followed by Gibbs sampling updates for the stick-breaking weights and atoms and the concentration hyperparameters for each local and global DP. The local distribution indicators z_{ij}^l , local distribution proportion π^l , AE signal strengths λ_{iJ} for the reference drug J , and zero-inflation indicators y_{ij} and probabilities ω_j (if included in the model) also admit standard Gibbs updates. However, the full conditionals for the DP base Gamma hyperparameters (β_j and β) and the reference category shrinkage hyperparameter τ lack standard forms; for these we employ stepping-out slice sampling (Neal, 2003). Detailed MCMC steps are provided in Supplementary Algorithms S.1, S.2 and S.3. For signal detection, we use an FDR-controlled, FNR-optimized hypothesis testing framework based on posterior draws for λ_{ij} , described next.

3.4 Signal detection using hypothesis testing

For signal detection we consider testing the hypotheses:

$$H_{0,ij} : \lambda_{ij} \leq 1 \text{ vs. } H_{1,ij} : \lambda_{ij} > 1$$

for all AEs $i = 1, \dots, I$ and all drugs $j = 1, \dots, J$. The null hypothesis $H_{0,ij}$ is rejected in favor of $H_{1,ij}$, identifying the drug- j and AE- i pair to be a signal, if $T_{ij} > k$, where T_{ij} is a test statistic derived from the posterior distribution and $k > 1$ is an appropriate threshold. A common choice for T_{ij} is the marginal posterior posterior quantile $T_{ij}(p)$, defined by $\Pr_{\text{posterior}}(\lambda_{ij} \leq T_{ij}(p)) = p$ for a small pre-specified quantile level $p \in (0, 1)$, where $\Pr_{\text{posterior}}(\cdot)$ denotes posterior probability given the data, and can be computed via MCMC draws. Hu et al. (2015) suggest using the 5-th posterior quantiles $T_{ij}(0.05)$ as the test statistic with a rejection threshold of $k = 2$; however, such deterministic thresholds can be overly conservative (curtailing sensitivity) or overly liberal (failing to control false discoveries). Instead, we consider a family of tests $\{T_{ij}(p) > k\}$ with varying p (reasonably small) and $k > 1$, selecting the optimal (\hat{p}, \hat{k}) that controls the false discovery rate (FDR) while minimizing the false negative rate (FNR). Given p and k , FDR and FNR are estimated using the posterior distribution as (Ahmed et al. 2010; Müller et al. 2006; in the expressions

below $1(A)$ denotes the indicator of a set A , $\hat{=}$ denotes “estimated by”, and T^{obs} is the computed value of T):

$$\text{FDR}(p, k) \hat{=} \frac{\sum_{i,j} q_{ij} I(T_{ij}(p)^{\text{obs}} > k)}{\sum_{i,j} 1(T_{ij}(p)^{\text{obs}} > k)}, \quad \text{FNR}(p, k) \hat{=} \frac{\sum_{i,j} (1 - q_{ij}) 1(T_{ij}(p)^{\text{obs}} \leq k)}{\sum_{i,j} 1(T_{ij}(p)^{\text{obs}} \leq k)}, \quad (4)$$

where $q_{ij} = \Pr_{\text{posterior}}(\lambda_{ij} \leq 1)$ is the posterior probability of $H_{0,ij}$, computable from MCMC draws. A grid search is used to determine the optimal (\hat{p}, \hat{k}) that ensures $\text{FDR}(\hat{p}, \hat{k}) \leq \alpha$ for a pre-specified level α while minimizing FNR (see Supplement S.3.3 for details on the grids).

In practice, drug-AE pairs with $n_{ij} = 1$ are often deemed non-signals, even if $\lambda_{ij} \gg 1$ with high posterior probability, leading to $T_{ij}(p) > k$ for suitably chosen p and k . To prevent their detection as signals, the rejection region can be modified to $\{T_{ij}(p) > k \text{ and } n_{ij} > 1\}$.

4 SIMULATION ASSESSMENTS

In this section, we conduct extensive simulations to assess the signal detection performance of our local-global DP Poisson and ZIP models under a wide array of data-generating settings. To generate random SRS contingency tables of dimension $I \times J$, we first define a prespecified *true* signal strength matrix (described below) $\Lambda^0 = ((\lambda_{ij}^0))$ encoding signals, structural zeros, non-signals, and between-drug dependency patterns. Using a reference $I \times J$ contingency table (described next) from a real-world SRS database, we extract row and column totals $\{\mathbf{n}_{i\bullet} : i = 1, \dots, I\}$ and $\{\mathbf{n}_{\bullet j} : j = 1, \dots, J\}$, respectively, to facilitate random contingency table generation. Next, we generate $\mathbf{p}_{i\bullet} \sim \text{Dirichlet}(\mathbf{n}_{i\bullet})$ and $\mathbf{p}_{\bullet j} \sim \text{Dirichlet}(\mathbf{n}_{\bullet j})$ for all i, j defining the random probability matrix $\mathbf{p} = ((p_{ij}))$ with $p_{ij} \propto \lambda_{ij}^0 \mathbf{p}_{i\bullet} \mathbf{p}_{\bullet j}$ and $\sum_{i,j} p_{ij} = 1$. Finally, we generate a random SRS contingency table by sampling from $\text{Multinomial}(\mathbf{n}_{\bullet\bullet}; \mathbf{p})$, collapsing any generated $n_{ij} = 1$ corresponding to a true signal (as defined by λ_{ij}^0) to $n_{ij} = 0$ afterward to eliminate signal detection at $n_{ij} = 1$.

Reference SRS dataset to compute row and column totals. We use the FDA FAERS database (Q3 2014-Q4 2020), which catalogs a total of 63,976,610 reported cases (Chakraborty et al., 2023), to construct our reference SRS contingency table. We focus on six statin medications: Atorvastatin, Fluvastatin, Lovastatin, Pravastatin, Rosuvastatin, and Simvastatin, collapsing all other drugs into a comparator “Other drugs” category. Using 46 preferred terms (PTs) for AEs, we form a 47×7 contingency table summarizing the report counts for each drug-AE pair. This dataset has been previously analyzed in Chakraborty et al. (2022).

Constructing the true signal strength matrix Λ^0 . To generate Λ^0 , we define two signal patterns: (1) *fixed row signals*, where all drugs (columns) exhibit signals for the same AEs (PTs; rows), and (2) *random signals*, where signals appear on randomly chosen AEs (different row for each drug). A larger number of fixed row signals increase the between-drug associations, measured via correlations between λ_{ij}^0 and $\lambda_{i'j'}^0$, for different statin drugs j and j' , while more random signals weaken them. The matrix Λ^0 is constructed by specifying fixed row signals and embedding additional random signals in the remaining rows across all statin columns. Signal strengths in these cells range from $1 < \lambda_{ij}^0 \leq 3$ (see Table 1). The remaining cells (i', j') are designated as non-signals with $\lambda_{i'j'}^0 = 1$. To introduce zero inflation, we prespecify *true* ω_j^0 (0 or 0.10; Table 1), and set $\omega_j^0 I$ randomly selected non-signal cells to $\lambda_{ij}^0 = 0$. This approach yields a controlled Λ^0 to generate random SRS contingency tables. Within this setup, we designed three simulation scenarios, each with and without zero-inflation (see Table 1).

Table 1: Simulation scenarios describing the construction of the true signal strength matrix Λ^0 encoding signals, non-signals, zero-inflation, and between-drug associations. The first two rows in the table show the number of fixed-AE/row signals and the number of random signals per (statin) column in Λ^0 . The zero inflation rate (third row in the table) shows the drug-specific true zero-inflation probability ω_j^0 in each simulation scenario. The comparator ‘‘Other drugs’’ column has all non-signal ($\lambda_{ij}^0 = 1$) cells. Finally, the fourth row in the table shows the average Pearson’s correlation coefficient ρ between λ_{ij}^0 and $\lambda_{i'j'}$, over all statin drug pairs j and j' (excluding the ‘‘Other drugs’’ category) as a measure of pairwise dependence between drugs.

Simulation Scenario	1a	1b	2a	2b	3a	3b
No. of fixed row signals	1	1	3	3	6	6
No. of random signals per column	5	5	3	3	1	1
Zero-inflation rate per column	0	0.1	0	0.1	0	0.1
Average ρ between columns	0.04	0.04	0.43	0.43	0.83	0.83

The common/fixed PTs (fixed AEs/rows) that are considered signal in each case are as follows:

- Case 1: Rhabdomyolysis
- Case 2: Muscle Disorder, Myalgia, Rhabdomyolysis
- Case 3: Blood Creatine Phosphokinase Increased, Muscle Disorder, Muscle Rupture, Musculoskeletal Discomfort, Myalgia, Rhabdomyolysis

A common signal strength value $\lambda^{0,\text{signal}}$ is assigned to all signal cells in a given simulation setting, and we vary $\lambda^{0,\text{signal}} \in \{1.1, 1.2, 1.3, 1.4, 1.5, 1.7, 1.9, 2, 2.5, 3\}$.

Replicated Data Generation, Model Fitting, and signal detection. For each constructed signal strength matrix Λ (Table 1), and using the random contingency table generation mechanism described earlier, we generate $R = 1,000$ independent random contingency table replicates. In each replicate, we fit our models via MCMC sampling (Supplementary Algorithms S.1, S.2 and S.3) with 10,000 post-burn-in draws after discarding the first 5,000 burn-in draws; see Supplement S.3 for additional computational details, including starting points. From the computed posteriors, we conduct signal detection using hypothesis testing (Section 3.4).

We compare our signal detection performance against existing Bayesian SRS data mining methods, viz., BCPNN, GPS, and the *local-only* DP model of Hu et al. (2015) (henceforth DP Hu et al.). For our models and DP Hu et al., signal detection uses an optimized posterior quantile level \hat{p} (fixed at 0.05 for DP Hu et al.) and threshold \hat{k} ensuring $\text{FDR} \leq 0.05$ while minimizing FNR (Section 3.4), with the additional constraint $n_{ij} > 1$ for our methods. To ensure fair FDR control (≤ 0.05) in BCPNN and GPS, we leverage the independence of signal strengths in the (empirical) Bayes posteriors for these two models and compute Benjamini-Hochberg-adjusted (Müller et al., 2006) posterior probabilities of being a non-signal; a drug- j and AE- i pair is then classified as a signal if the adjusted probability is ≤ 0.05 . Additionally, we evaluate the state-of-the-art frequentist ZIP-based extended (pseudo) LRT (Chakraborty et al., 2022; Huang et al., 2011; Ding et al., 2020), which ensures FDR control (≤ 0.05) with high

sensitivity while addressing zero inflation in the counts when present (see Supplement S.1 for a detailed review of competing approaches).

We assess signal detection for all methods using replication-based FDR, sensitivity, average Type I error, and F-score (Figure 3). For each method, these metrics are computed as $\text{FDR} = R^{-1} \sum_r (\text{FP}_r / (\text{FP}_r + \text{TP}_r))$, $\text{sensitivity} = R^{-1} \sum_r (\text{TP}_r / (\text{TP}_r + \text{FN}_r))$, $\text{average type I error} = R^{-1} \sum_r (\text{FP}_r / \text{TN}_r)$, and $\text{F-score} = R^{-1} \sum_r (2\text{TP}_r / (2\text{TP}_r + \text{FN}_r + \text{FP}_r))$ where TP_r and FN_r denote the number of *true signals* that are discovered and not discovered respectively, and FP_r and TN_r are the number of *true non-signals* discovered and not discovered in replicate r based on the signal strength values as cataloged in the corresponding *true* Λ .

The first two rows of Figure 3 show comparable (when $\lambda^{0,\text{signal}} < 1.5$) or slightly better (when $\lambda^{0,\text{signal}} \geq 1.5$) sensitivity for our local-global methods compared to all other methods when the between-drug association is near zero (Cases 1a,b). Under moderate between-drug association ($\rho = 0.43$; Cases 2a,b), our methods perform noticeably better in detecting more true signals, achieving up to twice the sensitivity, particularly for weak or moderate true signal strengths ($1.1 \leq \lambda^{0,\text{signal}} \leq 1.7$). The gain is even further pronounced under high between-drug association ($\rho = 0.83$; Cases 3a,b), where our methods attain sensitivities of ≥ 0.70 with only moderate true signal strength ($\lambda^{0,\text{signal}} \geq 1.7$), while all competitors fail to reach 0.70 sensitivity even for $\lambda^{0,\text{signal}} = 3$. These results highlight the substantial boost in signal detection from effectively leveraging between-drug similarities as facilitated by our models. In all settings, the FDR and average type I error is strictly controlled for all methods.

The Poisson and ZIP-based DP local-global models perform similarly across all scenarios regardless of the presence of zero-inflated observed counts (sub-cases a and b), due to the flexibility of the DP-based nonparametric framework (see Remark 3.1).

All computations were performed on the cluster computing facility at the Center for Computational Research at the University at Buffalo, with each process running on 16 GB RAM and a clock speed of 1.6-3 GHz. The median computation time per replication for our DP local-global methods (both Poisson and ZIP) was 145 seconds.

5 REAL DATA ANALYSIS

We use the statin data from Section 4 to demonstrate our method’s utility in real-world SRS data mining. Applying our DP local-global models (using the same MCMC and test statistic generation settings as used for simulated data analysis in Section 4) we compare detected signals against those from the DP Hu et al., BCPNN, GPS, and LRT. Table 2 presents the number of signals identified across statin drugs. The results indicate identical performance for our Poisson and ZIP models, detecting more signals than all competing methods.

To further examine the results, we focus on 20 PTs (AEs/ i) with the highest average (across statin drugs) posterior medians of λ_{ij} from our DP Poisson local-global model (Figure 4). The heatmap indicates non-detection (gray) or the degree of information sharing between drugs, measured via the posterior probabilities of $1 - z_{ij}^l$ (white-blue gradient; darker blue signifies greater information sharing at each AE). Our method detects several rare AEs with $n_{ij} = 2$, some also identified by certain competing methods (though no other method detects all these AEs simultaneously) and some not detected by any competing method (not shown in Figure 4; see Table 2). This, along with strong FDR control, highlights our method’s effectiveness in SRS signal detection.

Table 2: Summary table of discoveries from our proposed DP local-global models, and comparing them to the other existing methods. The count in each cell represents the number of AE signals detected by the method (along the columns), first separately for each drug and then in total (rows). The number of discoveries made uniquely by our DP Poisson local-global method but not by the other methods are presented in parentheses.

Drug	DP Poisson	DP ZIP	DP Hu et al.	BCPNN	GPS	LRT
Atorvastatin	33	33 (0)	33 (0)	28 (5)	26 (7)	28 (5)
Fluvastatin	14	14 (0)	13 (1)	10 (4)	12 (2)	12 (2)
Lovastatin	12	12 (0)	10 (2)	9 (3)	9 (3)	9 (3)
Pravastatin	23	23 (0)	17 (6)	11 (12)	11 (12)	11 (12)
Rosuvastatin	29	29 (0)	28 (1)	25 (4)	25 (4)	25 (4)
Simvastatin	29	29 (0)	28 (1)	26 (3)	25 (4)	25 (4)
Total	140	140 (0)	129 (11)	110 (31)	110 (32)	110 (30)

Finally, we focus on inferring structural zeros through the estimated drug-specific zero-inflation probabilities ω_j as returned by our DP ZIP local-global model. For comparison, we also monitor the corresponding estimates provided by the frequentist ZIP (pseudo) LRT method. The two methods yield largely similar results: our approach produces point estimates (posterior mean) for ω_j as 0.02, 0.10, 0.11, 0.08, 0.02, and 0.03 for Atorvastatin, Fluvastatin, Lovastatin, Pravastatin, Rosuvastatin, and Simvastatin, respectively. The corresponding frequentist maximum likelihood estimates are 0.00, 0.07, 0.16, 0.06, 0.00, and 0.00, respectively.

6 DISCUSSION

We propose nonparametric Bayesian models and their MCMC implementation for SRS data mining, balancing flexibility with shrinkage while capturing between-drug associations. Signal detection is performed through hypothesis tests that control FDR and minimize FNR, both estimated from MCMC posteriors. Our approach achieves significantly higher sensitivity than existing methods, particularly for rarer AEs and/or new drugs.

There are several limitations with our current approach that motivate interesting future directions. First, we focus here primarily on signal detection, i.e., to identify critical AEs of concern for each drug. The clusters of AEs produced by our DP priors have not been investigated but may reveal additional, deeper insights by identifying groups of “similar AEs”. A reformulation via mixed membership models could further enhance interpretability by allowing the same AE to appear in multiple clusters/groups. Second, while we consider data-driven characterization of similarities in AE signal strengths between drugs, a more flexible approach acknowledging known Drug-Drug Interactions (DDI; Poleksic and Xie 2019), possibly via appropriate prior distributions, may further enhance signal detection. Finally, our current framework aggregates drug-AE data across time points for a cross-sectional analysis. Extending the model to accommodate temporal variations in SRS data could enable formal identification of evolving AE patterns.

Acknowledgment. The authors are deeply grateful to Prof. Marianthi Markatou at the University at Buffalo for her insightful comments and helpful suggestions on the manuscript.

References

- Ahmed, I., Dalmasso, C., Haramburu, F., Thiessard, F., Broët, P., and Tubert-Bitter, P. (2010). False discovery rate estimation for frequentist pharmacovigilance signal detection methods. *Biometrics*, 66(1):301–309.
- Antoniak, C. E. (1974). Mixtures of Dirichlet processes with applications to Bayesian nonparametric problems. *The Annals of Statistics*, pages 1152–1174.
- Bate, A., Lindquist, M., Edwards, I. R., Olsson, S., Orre, R., Lansner, A., and De Freitas, R. M. (1998). A Bayesian neural network method for adverse drug reaction signal generation. *European Journal of Clinical Pharmacology*, 54:315–321.
- Bhadra, A., Datta, J., Polson, N. G., and Willard, B. (2019). Lasso meets horseshoe. *Statistical Science*, 34(3):405–427.
- Chakraborty, S., Liu, A., Ball, R., and Markatou, M. (2022). On the use of the likelihood ratio test methodology in pharmacovigilance. *Statistics in Medicine*, 41(27):5395–5420.
- Chakraborty, S., Markatou, M., and Ball, R. (2023). Likelihood ratio test-based drug safety assessment using R package pvLRT. *R Journal*, 15(1).
- Ding, Y., Markatou, M., and Ball, R. (2020). An evaluation of statistical approaches to postmarketing surveillance. *Statistics in Medicine*, 39(7):845–874.
- DuMouchel, W. (1999). Bayesian data mining in large frequency tables, with an application to the FDA spontaneous reporting system. *The American Statistician*, 53(3):177–190.
- DuMouchel, W. and Pregibon, D. (2001). Empirical Bayes screening for multi-item associations. In *Proceedings of the seventh ACM SIGKDD international conference on Knowledge Discovery and Data Mining*, pages 67–76.
- Evans, S. J., Waller, P. C., and Davis, S. (2001). Use of proportional reporting ratios (PRRs) for signal generation from spontaneous adverse drug reaction reports. *Pharmacoepidemiology and Drug Safety*, 10(6):483–486.
- Frühwirth-Schnatter, S. and Malsiner-Walli, G. (2019). From here to infinity: sparse finite versus Dirichlet process mixtures in model-based clustering. *Advances in Data Analysis and Classification*, 13:33–64.
- Hu, N., Huang, L., and Tiwari, R. C. (2015). Signal detection in FDA AERS database using Dirichlet process. *Statistics in Medicine*, 34(19):2725–2742.
- Huang, L., Zalkikar, J., and Tiwari, R. (2014). Likelihood ratio based tests for longitudinal drug safety data. *Statistics in Medicine*, 33(14):2408–2424.
- Huang, L., Zalkikar, J., and Tiwari, R. C. (2011). A likelihood ratio test based method for signal detection with application to FDA’s drug safety data. *Journal of the American Statistical Association*, 106(496):1230–1241.
- Huang, L., Zalkikar, J., and Tiwari, R. C. (2013). Likelihood ratio test-based method for signal detection in drug classes using FDA’s AERS database. *Journal of Biopharmaceutical Statistics*, 23(1):178–200.
- Ishwaran, H. and Zarepour, M. (2002). Exact and approximate sum representations for the Dirichlet process. *Canadian Journal of Statistics*, 30(2):269–283.
- Lavertu, A., Vora, B., Giacomini, K. M., Altman, R., and Rensi, S. (2021). A new era in pharmacovigilance: toward real-world data and digital monitoring. *Clinical Pharmacology & Therapeutics*, 109(5):1197–1202.

- Liu, A., Markatou, M., Chakraborty, S., and Ball, R. (2024). A pattern discovery algorithm for pharmacovigilance signal detection. Technical report, University at Buffalo.
- Markatou, M. and Ball, R. (2014). A pattern discovery framework for adverse event evaluation and inference in spontaneous reporting systems. *Statistical Analysis and Data Mining: The ASA Data Science Journal*, 7(5):352–367.
- Montastruc, J.-L. (2023). Rhabdomyolysis and statins: a pharmacovigilance comparative study between statins. *British Journal of Clinical Pharmacology*, 89(8):2636–2638.
- Müller, P., Parmigiani, G., and Rice, K. (2006). FDR and Bayesian Multiple Comparisons Rules. *Bayesian Statistics 8: Proceedings of the Eighth Valencia International Meeting June 2–6*.
- Neal, R. M. (2003). Slice sampling. *The Annals of Statistics*, 31(3):705–767.
- Plummer, M. et al. (2003). Jags: A program for analysis of Bayesian graphical models using Gibbs sampling. In *Proceedings of the 3rd international workshop on distributed statistical computing*, volume 124, pages 1–10. Vienna, Austria.
- Poleksic, A. and Xie, L. (2019). Database of adverse events associated with drugs and drug combinations. *Scientific Reports*, 9(1):20025.
- Polson, N. G. and Scott, J. G. (2012). On the Half-Cauchy Prior for a Global Scale Parameter. *Bayesian Analysis*, 7(4):887–902.
- Poluzzi, E., Raschi, E., Piccinni, C., and De Ponti, F. (2012). Data mining techniques in pharmacovigilance: analysis of the publicly accessible FDA adverse event reporting system (AERS). In *Data mining applications in engineering and medicine*. IntechOpen.
- Raschi, E., La Placa, M., Poluzzi, E., and De Ponti, F. (2021). The value of case reports and spontaneous reporting systems for pharmacovigilance and clinical practice. *British Journal of Dermatology*, 184(3):581–583.
- Rothman, K. J., Lanes, S., and Sacks, S. T. (2004). The reporting odds ratio and its advantages over the proportional reporting ratio. *Pharmacoepidemiology and Drug Safety*, 13(8):519–523.
- Sardella, M. and Belcher, G. (2018). Pharmacovigilance of medicines for rare and ultrarare diseases. *Therapeutic Advances in Drug Safety*, 9(11):631–638.
- Seneff, S. (2016). Statins and myoglobin: How muscle pain and weakness progress to heart, lung and kidney failure. *British Medical Bulletin*, 119(1):75.
- Sethuraman, J. (1994). A constructive definition of Dirichlet priors. *Statistica Sinica*, pages 639–650.
- Teh, Y., Jordan, M., Beal, M., and Blei, D. (2004). Sharing clusters among related groups: Hierarchical Dirichlet processes. In Saul, L., Weiss, Y., and Bottou, L., editors, *Advances in Neural Information Processing Systems*, volume 17. MIT Press.

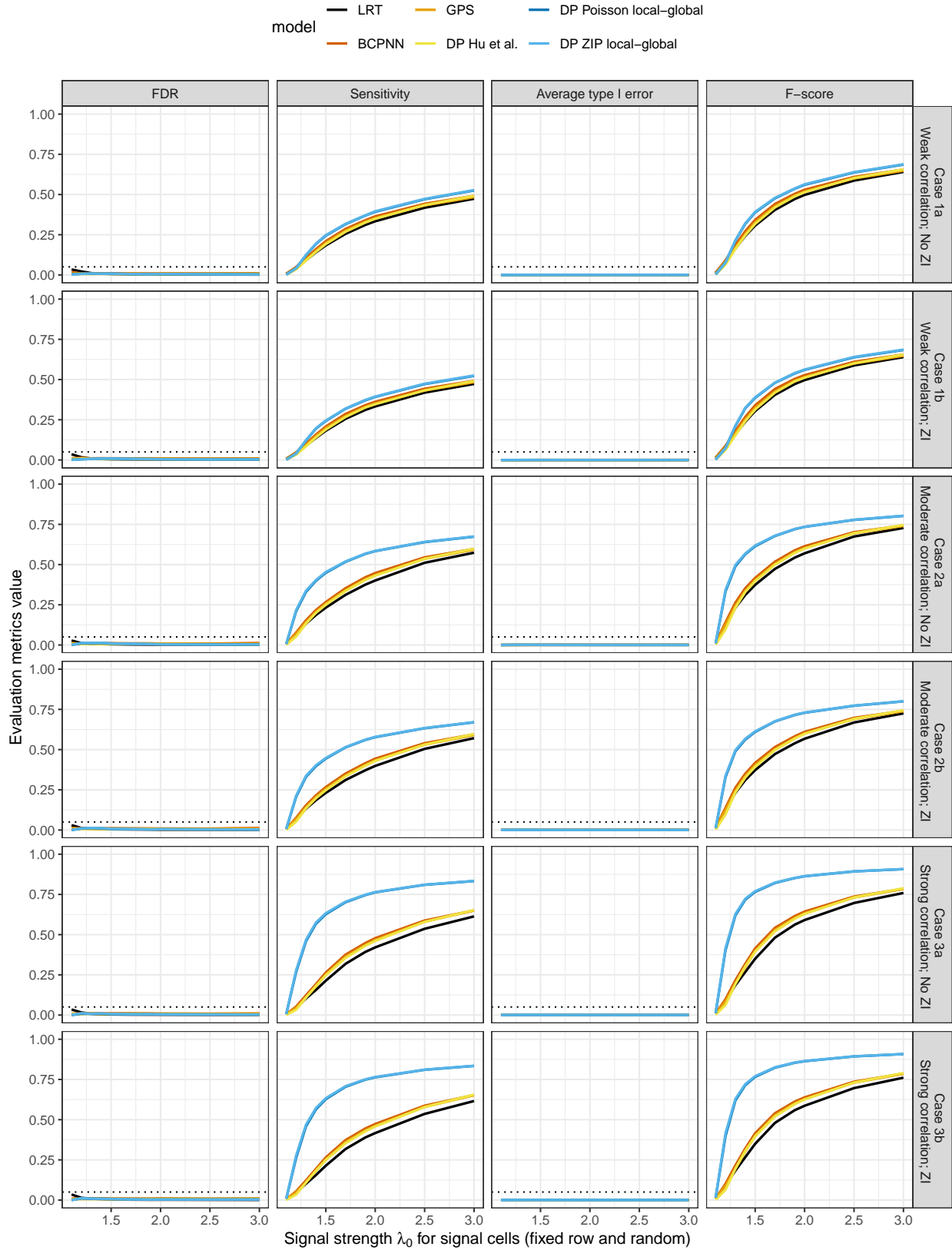


Figure 3: Simulation results: the horizontal axis shows the true signal strength λ_0 for signal cells, the vertical axis shows the value of evaluation metrics. Each column presents one metric and each row presents one simulation scenario in Table 1.

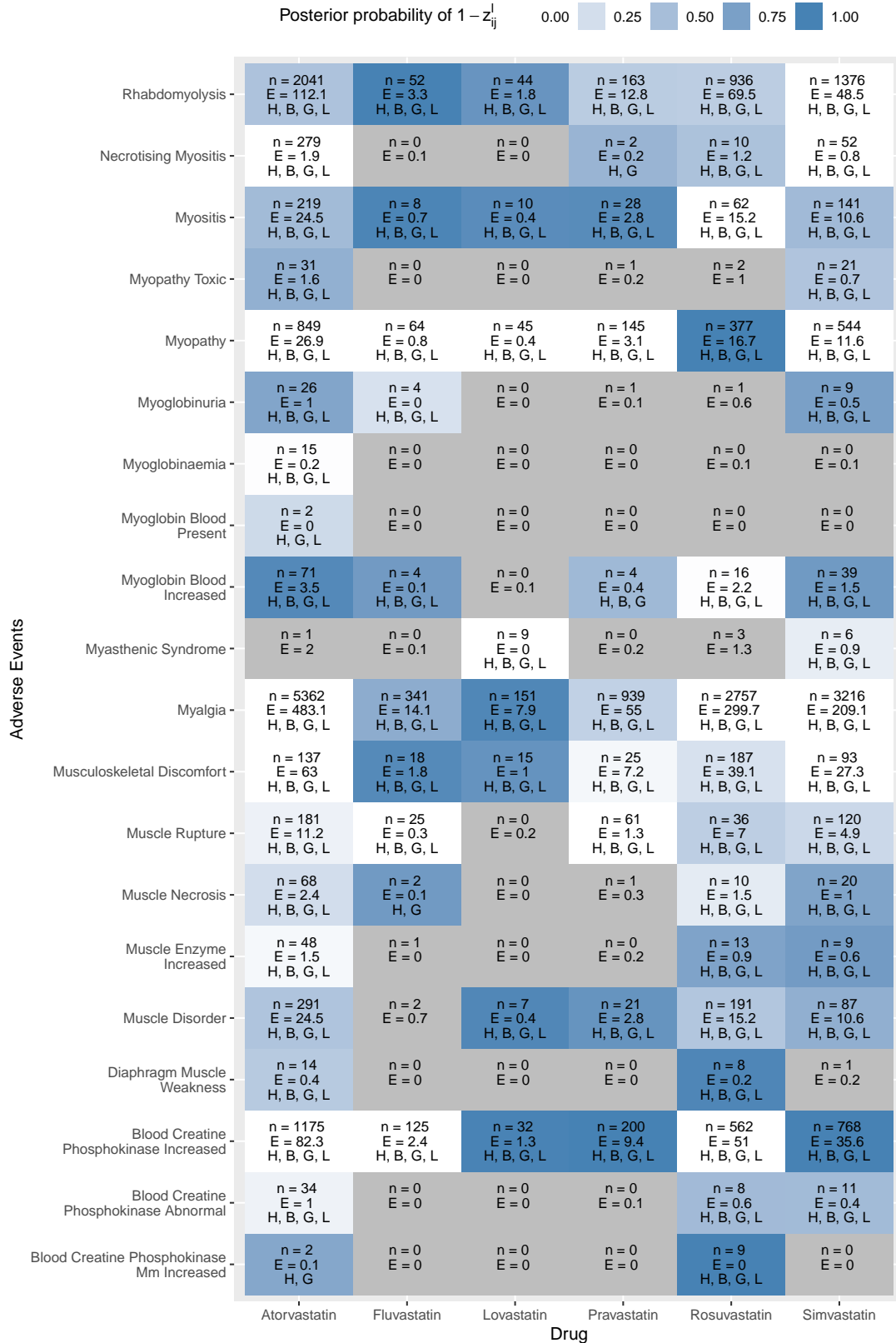


Figure 4: Heatmap of 20 selected PTs. Cells not detected as signals by our method are colored gray. White-to-blue shades represent the posterior probability of $1 - z_{ij}^l$, with darker (lighter) blue indicating a higher (lower) probability that the signal strength originates from the global signal strength distribution. The letters “H”, “B”, “G”, and “L” indicate signal detection by the DP Hu et al., BCPNN, GPS, and likelihood ratio test, respectively.

Supplementary Material

This supplement provides a brief review of existing SRS data mining methods, additional details about the DP local-global models, detailed steps for the MCMC algorithms implementing our models, additional computation details, and additional simulation results. Sections, tables, and figures in this supplement are labeled with a prefix ‘‘S.’’, such as, Section S.1, Table S.1, and Figure S.1, etc.

S.1 A REVIEW OF EXISTING BAYESIAN/EMPIRICAL BAYESIAN SRS DATA MINING METHODS AND THE ZIP MODEL-BASED LIKELIHOOD RATIO TEST METHOD

S.1.1 The GPS model

The GPS method (DuMouchel, 1999) employs an empirical Bayes approach for stabilized signal detection within a Poisson model-based framework for the report counts n_{ij} . Specifically, we assume $n_{ij} \sim \text{Poisson}(E_{ij}\lambda_{ij})$, with λ_{ij} parametrizing the signal strength for the drug- j and AE- i pair. A two-component gamma mixture prior for λ_{ij} is considered:

$$\lambda_{ij} \sim \kappa \text{Gamma}(\alpha_1, \beta_1) + (1 - \kappa) \text{Gamma}(\alpha_2, \beta_2),$$

where $\kappa \in [0, 1]$ is the mixing weight hyperparameter, and $\alpha_1, \beta_1 > 0$, and $\alpha_2, \beta_2 > 0$ are mixture component-specific gamma hyperparameters. Here $\text{Gamma}(\alpha, \beta)$ denotes a probability distribution with density $f_{\text{gamma}}(y | \alpha, \beta) = \frac{1}{\Gamma(\alpha)} \beta^\alpha y^{\alpha-1} e^{-\beta y}$, $y > 0$; $\alpha, \beta > 0$. The posterior distribution of λ_{ij} given n_{ij} , E_{ij} , and the hyperparameters is:

$$\lambda_{ij} | n_{ij}, E_{ij} \sim \kappa_{ij} \text{Gamma}(\hat{\alpha}_1 + n_{ij}, \hat{\beta}_1 + E_{ij}) + (1 - \kappa_{ij}) \text{Gamma}(\hat{\alpha}_2 + n_{ij}, \hat{\beta}_2 + E_{ij})$$

where $\kappa_{ij} = \kappa f_{\text{Gamma}}(\lambda_{ij} | \alpha_1, \beta_1) / [\kappa f_{\text{Gamma}}(\lambda_{ij} | \alpha_1, \beta_1) + (1 - \kappa) f_{\text{Gamma}}(\lambda_{ij} | \alpha_2, \beta_2)]$. Under an empirical Bayes approach, the point estimates $\hat{\kappa}$, $\hat{\alpha}_1$, $\hat{\beta}_1$, $\hat{\alpha}_2$, and $\hat{\beta}_2$ for the hyperparameters are obtained by maximizing their marginal likelihoods given n_{ij} and E_{ij} . The resulting posterior of λ_{ij} conditional on these estimated hyperparameters is used for inference and signal detection. Specifically, DuMouchel and Pregibon (2001) define the empirical Bayesian score $E(\log_2(\lambda_{ij}) | n_{ij}, E_{ij}, \hat{\kappa}, \hat{\alpha}_1, \hat{\beta}_1, \hat{\alpha}_2, \hat{\beta}_2)$ as a point estimate of signal strength for the drug- j and AE- i pair, and also suggest determining the pair to be a signal if the 5th percentile (EB05) of the above conditional posterior for λ_{ij} exceeds 2.

S.1.2 The BCPNN method

The BCPNN approach (Bate et al., 1998) assumes that conditional on the grand total count $n_{\bullet\bullet}$, the cell-specific counts n_{ij} , the marginal row totals $n_{i\bullet}$, and the marginal column totals $n_{\bullet j}$ each distributed as binomial-beta: (a) $n_{ij} | p_{ij} \sim \text{Binomial}(n_{\bullet\bullet}, p_{ij})$, $p_{ij} \sim \text{Beta}(\alpha_{ij}, \beta_{ij})$, (b) $n_{i\bullet} | p_{i\bullet} \sim \text{Binomial}(n_{\bullet\bullet}, p_{i\bullet})$, $p_{i\bullet} \sim \text{Beta}(\alpha_{i\bullet}, \beta_{i\bullet})$, (c) $n_{\bullet j} | p_{\bullet j} \sim \text{Binomial}(n_{\bullet\bullet}, p_{\bullet j})$, $p_{\bullet j} \sim \text{Beta}(\alpha_{\bullet j}, \beta_{\bullet j})$, where p_{ij} is the cell reporting rate, and $p_{i\bullet}$ and $p_{\bullet j}$ are the marginal row and column reporting rates. (Note that the binomial model assumptions for n_{ij} , $n_{i\bullet}$ and $n_{\bullet j}$ can be understood as consequences of an independent Poisson model for n_{ij} with certain choices of p_{ij} , $p_{i\bullet}$, and $p_{\bullet j}$.) Bate et al. (1998) consider the information content $\text{IC}_{ij} = \log_2 [p_{ij} / (p_{i\bullet} p_{\bullet j})]$ as a measure of signal strength for the drug- j

AE- i pair, with a higher IC indicating a stronger association. The authors suggest an empirical Bayes estimation of these quantities using $\hat{\alpha}_{ij} = \hat{\alpha}_{i\bullet} = \hat{\beta}_{i\bullet} = \hat{\alpha}_{\bullet j} = \hat{\beta}_{\bullet j} = 1$ and $\hat{\beta}_{ij} = 1/(E(p_{i\bullet} | n_{i\bullet})E(p_{\bullet j} | n_{\bullet j})) - 1$, with the denominator of $\hat{\beta}_{ij}$ being computed using the posterior distributions $p_{i\bullet} | n_{i\bullet} \sim \text{Beta}(\hat{\alpha}_{i\bullet} + n_{i\bullet}, \hat{\beta}_{i\bullet} + n_{\bullet\bullet} - n_{i\bullet})$ and $p_{\bullet j} | n_{\bullet j} \sim \text{Beta}(\hat{\alpha}_{\bullet j} + n_{\bullet j}, \hat{\beta}_{\bullet j} + n_{\bullet\bullet} - n_{\bullet j})$. The consequent (empirical Bayes) posterior distribution of IC_{ij} can be approximated using Monte Carlo simulation or an asymptotic normal distribution. A signal is detected at the drug- j and AE- i pair if the 2.5th posterior percentile for IC_{ij} exceeds 0.

S.1.3 DP Poisson method of Hu et al. (2015)

Hu et al. (2015) consider the same likelihood $n_{ij} \sim \text{Poisson}(\lambda_{ij}E_{ij})$ as in GPS, but extend the two-gamma mixture prior for λ_{ij} to a DP (infinite) mixture prior:

$$\lambda_{ij} | (\alpha_j, M_{0j}) \sim \text{DP}(\alpha, M_{0j}) = \sum_{h=1}^{\infty} \eta_{hj} \delta_{\{\theta_{hj}\}}$$

where the base distribution $M_{0j} \equiv \text{Gamma}(a_j, a_j)$ generates $\theta_{hj} \sim M_{0j}$ and the concentration hyperparameter $\alpha > 0$ generates the mixture weights $\{\eta_{hj}\}_{h=1}^{\infty}$ satisfying $\sum_{h=1}^{\infty} \eta_{hj} = 1$ with

$$\eta_{1j} = v_{1j}, \eta_{hj} = v_{hj} \prod_{t=1}^{h-1} (1 - v_{tj}), h = 2, \dots; v_{hj} \sim \text{independent Beta}(1, \alpha) \text{ for } h = 1, \dots \quad (5)$$

leveraging a stick-breaking representation (Sethuraman, 1994) for each j . Hu et al. (2015) consider full Bayesian inference on λ_{ij} by first eliciting a prior distribution on the hyperparameters a_j and α_j —specifically, independent vague priors $a_j \sim \text{Uniform}(0, 1)$ and $\alpha_j \sim \text{Uniform}(0.2, 10)$; $j = 1, \dots, J$ —and then utilizing MCMC sampling from the resulting joint posterior. Using MCMC posterior draws for λ_{ij} , a signal at the drug- j and AE- i pair is identified if the 5th posterior percentile of λ_{ij} exceeds a threshold of 2.

S.1.4 ZIP model based Pseudo LRT (frequentist) method

The likelihood ratio test based method and its variants (Huang et al., 2011, 2013, 2014) have an advantage in FDR control while maintaining high sensitivity. Additionally, the use of a post-hoc threshold makes it more suitable for practical applications. Consider the reporting count $n_{ij} \sim \text{ZIP}(n = n_{ij} | \lambda_{ij} \times E_{ij}, \omega_j)$, where λ_{ij} is the relative reporting rate and $E_{ij} = n_{i\bullet}n_{\bullet j}/n_{\bullet\bullet}$ represents the expected count under independence. The pseudo LRT, as proposed by Chakraborty et al. (2022), is a recent method designed to accommodate the zero-inflated nature of SRS data while easing computational demands. Similar to the standard LRT method, this approach first tests a global alternative hypothesis $H_{aj} : \lambda_{ij} > 1$ for at least one $i \in \{1, \dots, I\}$ against the null hypothesis $H_{0j} : \lambda_{ij} = 1$ for all $i \in \{1, \dots, I\}$ for a given drug- j . If H_{aj} is rejected, a step-down procedure is used to conduct individual tests on $H_{aij} : \lambda_{ij} > 1$.

The ordinary LRT methods estimate the nuisance parameter ω_j from H_{0j} and $H_{0j} \cup H_{aj}$ individually, the pseudo LRT is constructed using a global estimate $\hat{\omega}_j$ of ω_j consistent under $H_{0j} \cup H_{aj}$ in both the numerator and the denominator of the likelihood ratio test statistic. The resulting statistic is given by

$$\text{LR}_{ij} = \exp(-(\hat{\lambda}_{ij} - 1)E_{ij})\hat{\lambda}_{ij}^{n_{ij}}.$$

The maximum likelihood ratio statistic for drug- j is then defined as $\text{MLR}_j = \max_{i \in \{1, \dots, I\}} \text{LR}_{ij}$. In the global test, a parametric bootstrap can be used to approximate the p-value $P_j = \Pr(\text{MLR}_j \geq \text{MLR}_j^{\text{obs}})$ using (parametric

bootstrap) draws for LR_{ij} under H_{0j} and hence MLR_j , where $\text{MLR}_j^{\text{obs}}$ is the observed test statistic. If the global test is rejected, the step-down p-values can be computed for the individual tests using the *same* parametric bootstrap samples for MLR_j and using the individual observed likelihood ratio test statistic values, such that $P_{ij} = \Pr(\text{LR}_{ij} \geq \text{MLR}_{ij}^{\text{obs}})$. For multiple drugs, the same approach can be applied, defining an overall maximum likelihood ratio as $\text{MLR} = \max_{i \in \{1, \dots, I\}, j \in \{1, \dots, J\}} \text{LR}_{ij}$. This step-down procedure avoids α -inflation by using the same global test statistic, thus controlling the false discovery rate at the α level.

A consistent estimate of ω_j is obtained by maximizing the profile likelihood $\ell_j(\omega_j)$, with $\hat{\lambda}_{ij} = \max\{1, n/E_{ij}\}$ as the MLE of λ_{ij} . The inference on zero-inflation is based on the estimate $\hat{\eta}_{ij}(\lambda_{ij}, \hat{\omega}_j) = \frac{\hat{\omega}_j}{\hat{\omega}_j + (1 - \hat{\omega}_j) \exp(-\lambda_{ij} E_{ij})}$, representing the estimated probability of zero-inflation for cells with zero count. A prediction of the zero-inflation indicator z_{ij} can be made by generating Bernoulli samples from $\hat{\eta}_{ij}$.

S.2 ADDITIONAL DETAILS FOR THE DP LOCAL-GLOBAL FRAMEWORK

In this section, we generalize the model to encompass different variants depending on the direction of information sharing. Moreover, we provide additional details of the DP local-global framework. And we propose a simpler shrinkage model as an alternative for the ‘‘Other drugs’’ as described in Section 3.2.

S.2.1 Complete hierarchical Bayesian representation of our models

In Section 3.2 in the main text, we present the concept of the DP Poisson local-global model. The fully formulated hierarchical representations are provided in the following two sections for the DP Poisson and the DP ZIP local-global model.

S.2.1.1 DP Poisson local-global model

A hierarchical representation of the complete model, including vague priors for the hyperparameters, is presented as follows.

likelihood:

$$n_{ij} \sim \text{Poisson}(\lambda_{ij} E_{ij})$$

DP local-global prior for a non-baseline drug $j \in \{1, \dots, J-1\}$:

$$\begin{aligned} \lambda_{ij} &\sim z_{ij}^l \lambda_{ij}^l + (1 - z_{ij}^l) \lambda_i^g \\ \lambda_{ij}^l &\sim D_j; \lambda_i^g \sim D \\ z_{ij}^l &\sim \text{Bernoulli}(\pi^l) \end{aligned}$$

DP local prior for drug- j :

$$\begin{aligned} D_j &\equiv \sum_{h=1}^{\infty} \eta_{hj} \delta_{\{\theta_{hj}\}} \approx \sum_{h=1}^K \eta_{hj} \delta_{\{\theta_{hj}\}} \sim \text{DP}(\alpha_j, G(\beta_j)) \\ \theta_{hj} &\sim G(\beta_j) \equiv \text{Gamma}(\text{shape} = \beta_j, \text{rate} = \beta_j) \\ \eta_{1j} &= v_{1j}, \eta_{hj} = v_{hj} \prod_{t=1}^{h-1} (1 - v_{tj}), h \geq 2 \\ v_{hj} &\sim \text{Beta}(1, \alpha_j), h = 1, \dots, K-1; v_{Kj} = 1 \end{aligned}$$

DP global prior:

$$\begin{aligned} D &\equiv \sum_{h=1}^{\infty} \eta_h \delta_{\{\theta_h\}} \approx \sum_{h=1}^K \eta_h \delta_{\{\theta_h\}} \sim \text{DP}(\alpha, G(\beta)) \\ \theta_h &\sim G(\beta) \equiv \text{Gamma}(\text{shape} = \beta, \text{rate} = \beta) \\ \eta_1 &= v_1, \eta_h = v_h \prod_{t=1}^{h-1} (1 - v_t), h \geq 2 \\ v_h &\sim \text{Beta}(1, \alpha) \end{aligned}$$

Gamma shrinkage prior for a baseline drug- J :

$$\lambda_{iJ} \sim \text{Gamma}(\text{shape} = \tau, \text{rate} = \tau)$$

vague proper priors for hyperparameters:

$$\begin{aligned} \pi^g &\sim \text{Uniform}(0, 1) \\ \alpha_j, \alpha &\sim \text{Gamma}(\text{shape} = 1, \text{rate} = 3) \\ \beta_j, \beta &\sim \text{Cauchy}^+(0, 0.5) \\ \tau &\sim \text{Cauchy}^+(0, 0.5) \end{aligned}$$

S.2.1.2 DP ZIP local-global model

A hierarchical representation of the complete model, including vague priors for the hyperparameters, is presented as follows.

likelihood:

$$\begin{aligned} n_{ij} &\sim y \text{Poisson}(\lambda_{ij} E_{ij}) + (1 - y) \delta_{\{0\}} \\ y &\sim \text{Bernoulli}(\omega_j) \end{aligned}$$

DP local-global prior for a non-baseline drug $j \in \{1, \dots, J - 1\}$:

$$\begin{aligned} \lambda_{ij} &\sim z_{ij}^l \lambda_{ij}^l + (1 - z_{ij}^l) \lambda_i^g \\ \lambda_{ij}^l &\sim D_j; \lambda_i^g \sim D \\ z_{ij}^l &\sim \text{Bernoulli}(\pi^l) \end{aligned}$$

DP local prior for drug- j :

$$\begin{aligned} D_j &\equiv DP(\alpha_j, G(\beta_j)) \equiv \sum_{h=1}^{\infty} \eta_{hj} \delta_{\{\theta_{hj}\}} \approx \sum_{h=1}^K \eta_{hj} \delta_{\{\theta_{hj}\}} \\ \theta_{hj} &\sim G_{0j} \equiv \text{Gamma}(\text{shape} = \beta_j, \text{rate} = \beta_j) \\ \eta_{1j} &= v_{1j}, \eta_{hj} = v_{hj} \prod_{t=1}^{h-1} (1 - v_{tj}), h \geq 2 \\ v_{hj} &\sim \text{Beta}(1, \alpha_j); v_{Kj} = 1 \end{aligned}$$

DP global prior:

$$\begin{aligned} D &\equiv DP(\alpha, G(\beta)) \equiv \sum_{h=1}^{\infty} \eta_h \delta_{\{\theta_h\}} \approx \sum_{h=1}^K \eta_h \delta_{\{\theta_h\}} \\ \theta_h &\sim G_0 \equiv \text{Gamma}(\beta, \beta) \\ \eta_1 &= v_1, \eta_h = v_h \prod_{t=1}^{h-1} (1 - v_t), h \geq 2 \\ v_h &\sim \text{Beta}(1, \alpha) \end{aligned}$$

Gamma shrinkage prior for a baseline drug- J :

$$\lambda_{iJ} \sim \text{Gamma}(\text{shape} = \tau, \text{rate} = \tau)$$

vague proper priors for hyperparameters:

$$\begin{aligned} \pi^g &\sim \text{Uniform}(0, 1) \\ \alpha_j, \alpha &\sim \text{Gamma}(\text{shape} = 1, \text{rate} = 3) \\ \beta_j, \beta &\sim \text{Cauchy}^+(0, 0.5) \\ \tau &\sim \text{Cauchy}^+(0, 0.5) \end{aligned}$$

S.2.2 Some notes on the ‘‘global-only’’ model

A special case of our local-global models leads to a reduced ‘‘global-only’’ model when $\pi^g = 0$, i.e., $\lambda_{ij} = \lambda_i^g$ for $j = 1, \dots, J - 1$. Under this model there is no provision for different λ_{ij} for any $j \neq J$. The global model has a simplified likelihood $n_{ij} \sim \text{Poisson}(\lambda_i E_{ij})$ here $\lambda_i^g \sim D$ if $j \neq J$, which produces $\sum_{j=1}^{J-1} n_{ij} \sim \text{Poisson}(\lambda_i \sum_{j=1}^{J-1} E_{ij})$. The

model reduction also impacts the signal detection. For the local-global framework, hypothesis testing is conducted for each individual λ_{ij} . On the other hand, under the global model, the test is simplified to evaluating whether $\lambda_i^g > 1$. Testing $\lambda_i^g > 1$ entails assessing if the summarized Poisson count $\sum_i n_{ij}$ is large compared to the expected count $\sum_i E_{ij}$, owing to the reduced model. This approach represents a “global test”, whereas our proposed local-global model allows conducting hypothesis testing for each individual drug-AE pair. As a result, directly comparing the global model with the local-global model is not feasible, as they target different types of assessment.

S.3 COMPUTATIONAL DETAILS

In this section, we first provide MCMC algorithms implementing our models in Section S.3.1. The MCMC algorithms are derived using finite mixture approximation of the underlying DP processes (Ishwaran and Zarepour, 2002; Frühwirth-Schnatter and Malsiner-Walli, 2019), and combine Gibbs sampling updates with stepping-out slice sampling updates (Neal, 2003) for various parameters. Some additional notes on the MCMC implementation, including initial value generation for our MCMC algorithms are then provided in Section S.3.2. Next we provide detailed notes on the grid-search method identifying optimal quantile-level p and threshold k used for our hypothesis tests for signal detection (Section S.3.3). The JAGS code (Plummer et al., 2003) for Hu et al. (2015)’s models is shown as a reference in Section S.1.3. The example statin dataset is included in Section S.3.5.

In our notation below, $\text{DPSB}_K(\boldsymbol{\eta} = (\eta_1, \dots, \eta_K), \boldsymbol{\theta} = (\theta_1, \dots, \theta_K), \alpha, \beta)$ denotes parameters associated with the model $\sum_{h=1}^K \eta_h 1_{\{\theta_h\}} \sim \text{DP}(\alpha, G(\beta))$, comprising the stick-breaking weights $\boldsymbol{\eta} = (\eta_1, \dots, \eta_K)$ and atoms $\boldsymbol{\theta} = (\theta_1, \dots, \theta_K)$ and DP concentration hyperparameter α and base (gamma) distribution hyperparameter β .

S.3.1 MCMC algorithms

S.3.2 Initial value generation for the MCMC algorithms

Given the observed data n_{ij} and E_{ij} for $i = 1, \dots, I$, $j = 1, \dots, J$, and a prespecified number K of DP mixture components for finite approximation, we initialize the number of nonempty components K_+ to the smallest integer greater than $\min\{K/2, I - 1\}$. The local-global indicators z_{ij}^l are randomly initialized by independently sampling each cell (i, j) from a Bernoulli(0.5) distribution. The DP parameters for each local and global DP process are then initialized using the subset of data (n_{ij}, E_{ij}) assigned to that process, as determined by the indicators z_{ij}^l , for $i = 1, \dots, J - 1$.

For the initialization of parameters in the local DP prior for the j -th drug ($j = 1, \dots, J - 1$), we perform k -means clustering with the initialized K_+ number of clusters on the set $(n_{ij} + 0.5)/(E_{ij} + 0.5) : z_{ij} = 1, i = 1, \dots, I$, and use the resulting cluster centers as initial values for the atoms θ_{hj} , $h = 1, \dots, K_+$, of the non-empty clusters. The probability weights η_{hj} for these non-empty clusters are initialized using the relative frequencies of the k -means clusters, and the clusters are then relabeled to ensure $\eta_{1j} \geq \eta_{2j} \geq \dots \geq \eta_{K_+j}$. These atoms θ_{hj} are then used for numerical maximum likelihood estimation of β with the model $\theta_{1j}, \dots, \theta_{K_+j} \sim \text{independent Gamma}(\text{shape} = \beta, \text{rate} = \beta)$, and the resulting estimate $\hat{\beta}$ is used to initialize β_j . The atoms $\theta_{h'j}$ for the remaining empty clusters ($h' = K_+ + 1, \dots, K$) are randomly drawn from $\text{Gamma}(\text{shape} = \beta_j, \text{rate} = \beta_j)$ using the initialized β_j . Their corresponding weights $\eta_{h'j}$ are initialized to $(\min_{h' \in 1, \dots, K_+} \eta_{h'j})/10$, and all weights η_{hj} for $h = 1, \dots, K$ are

Algorithm S.1 One Iteration of the MCMC algorithm updating $\text{DPSB}_K(\boldsymbol{\eta}, \boldsymbol{\theta}, \alpha, \beta)$ parameters from its posterior given data (n_i, E_i, z_i) under the model: $n_i \sim \text{Pois}(\lambda_i E_i)$, $\lambda_i \sim \text{DPSB}_K(\boldsymbol{\eta}, \boldsymbol{\theta}, \alpha, \beta)$, $\alpha \sim \text{Exponential}(\text{rate} = \psi_\alpha)$, $\beta \sim \pi_\beta(\beta)$, and z_i indicating if observation i contributes to the model ($z_i = 1$) or not ($z_i = 0$); $i = 1, \dots, N$.

1. Generate allocations $\mathbf{S} = (S_1, \dots, S_N)$ using

$$P(S_i = h \mid \boldsymbol{\eta}, \boldsymbol{\theta}, \mathbf{z}, \mathbf{n}, \mathbf{E}) = \frac{\eta_h \{f_{\text{Poisson}}(n_i \mid \theta_h E_i)\}^{z_i}}{\sum_{h'=1}^K \eta_{h'} \{f_{\text{Poisson}}(n_i \mid \theta_{h'} E_i)\}^{z_i}}$$

for $h = 1, \dots, K$. Here $f_{\text{Poisson}}(n \mid \theta)$ denotes the probability mass function of the Poisson(θ) distribution evaluated at n .

2. Generate $\theta_1, \dots, \theta_K$ independently from

$$\theta_h \mid \mathbf{S}, \alpha, \mathbf{n}, \mathbf{E}, \mathbf{z} \sim \text{Gamma}\left(\text{shape} = \sum_{i=1}^N n_i z_i 1(S_i = h) + \alpha, \text{rate} = \sum_{i=1}^N E_i z_i 1(S_i = h) + \alpha\right)$$

- 2.1. Calculate $\lambda_i = \theta_{S_i}$, $i = 1, \dots, N$

3. Generate β from the density

$$\pi(\beta \mid \boldsymbol{\theta}) \propto \prod_{h=1}^K f_{\text{Gamma}}(\theta_h \mid \text{shape} = \beta, \text{rate} = \beta) \pi_\beta(\beta)$$

Here $f_{\text{Gamma}}(\theta \mid \text{shape} = \beta, \text{rate} = \beta)$ denotes the probability density function of the Gamma(β, β) distribution at θ . $\pi(\beta)$ is the prior distribution of β . Direct random sampling from this density is not feasible. Instead, we use stepping-out slice sampling (Neal, 2003) to generate Markov chain draws for β .

4. Generate v_1, \dots, v_{K-1} independently from:

$$v_h \mid \mathbf{S}, \alpha \sim \text{Beta}\left(1 + \sum_{i=1}^N 1(S_i = h), \alpha + \sum_{i=1}^N 1(S_i > h)\right).$$

Then set $v_K = 1$ and calculate η_1, \dots, η_K from v_1, \dots, v_K using

$$\eta_1 = v_1, \quad \eta_h = v_h \prod_{t=1}^{h-1} (1 - v_t), \quad h = 2, \dots, K.$$

5. Generate α from

$$\alpha \mid v_1, \dots, v_K \sim \text{Gamma}\left(\text{shape} = K, \text{rate} = - \sum_{h=1}^{K-1} \log(1 - v_h) + \psi_\alpha\right).$$

Algorithm S.2 One Step Iteration of DP Poisson local-global column model (Given data $\{(n_{ij}, E_{ij}, z_{ij}^l) : i = 1, \dots, I; j = 1, \dots, J\}$)

1. Generate global $\text{DPSB}_K(\boldsymbol{\eta}, \boldsymbol{\theta}, \alpha, \beta)$ parameters using Algorithm S.1, with $\{(\tilde{n}_i, \tilde{E}_i, 1(\sum_{j=1}^{J-1} z_{ij}^l < J-1)) : i = 1, \dots, I\}$ as data where

$$\tilde{n}_j = \sum_{i=1}^{J-1} n_{ij}(1 - z_{ij}^l), \quad \tilde{E}_j = \sum_{i=1}^{J-1} E_{ij}(1 - z_{ij}^l).$$

- 1.1. Set $\lambda_i^g = \lambda_i$ returned from Algorithm S.1.
2. For $j = 1, \dots, J-1$, generate local $\text{DPSB}(\boldsymbol{\eta}_j, \boldsymbol{\theta}_j, \alpha_j, \beta_j)$ using Algorithm S.1 using $\{(n_{ij}, E_{ij}, z_{ij}^l); i = 1, \dots, I\}$ as data.
 - 2.1.j For this j , set $\lambda_{ij}^l = \lambda_i$ returned from Algorithm S.1.
3. Generate “local” allocations:

$$z_{ij}^l \mid n_{ij}, E_{ij}, z_{ij}^l, \lambda_{ij}^l, \lambda_i^g \sim \text{Bernoulli}(p_{ij}^l),$$

where

$$p_{ij}^l = \frac{\pi^l f_{\text{Poisson}}(n_{ij} \mid \lambda_{ij}^l E_{ij})}{f_{\text{Poisson}}(n_{ij} \mid \lambda_{ij}^l E_{ij}) + (1 - \pi^l) f_{\text{Poisson}}(n_{ij} \mid \lambda_i^g E_{ij})}.$$

4. Define $\lambda_{ij} = z_{ij}^l \lambda_{ij}^l + (1 - z_{ij}^l) \lambda_i^g$ for all $i = 1, \dots, I$ and $j = 1, \dots, (J-1)$.
5. Generate π^l using:

$$\pi^l \mid z_{ij}^l \sim \text{Beta} \left(a^l + \sum_{i=1}^I \sum_{j=1}^{J-1} z_{ij}^l, b^l + \sum_{i=1}^I \sum_{j=1}^{J-1} (1 - z_{ij}^l) \right),$$

Notes: $a^l = 1, b^l = 1$

6. Generate $\lambda_{1J}, \dots, \lambda_{IJ}$ from:

$$\lambda_{iJ} \mid \tau, n_{iJ}, E_{iJ} \sim \text{Gamma}(\text{shape} = n_{iJ} + \tau, \text{rate} = E_{iJ} + \tau).$$

7. Generate β_J from:

$$\pi(\beta_J \mid \lambda_{1J}, \dots, \lambda_{IJ}) \propto \prod_{i=1}^I f_{\text{Gamma}}(\lambda_{ij} \mid \text{shape} = \tau, \text{rate} = \tau) \pi_{\tau}(\tau).$$

Algorithm S.3 One Iteration of DP ZIP local-global Model Given data $(n_{ij}, E_{ij}, z_{ij}^l)$

1. Generate the ZI indicator y_{ij} for $i = 1, \dots, I, j = 1, \dots, J$, where:

$$y_{ij} \mid \omega_j, \lambda_{ij}, n_{ij}, E_{ij} \sim \text{Bernoulli}(p_{ij}^{\text{ZI}}),$$

where

$$p_{ij}^{\text{ZI}} = \begin{cases} \frac{\omega_j}{\omega_j + (1-\omega_j) \exp(-\lambda_{ij} E_{ij})}, & \text{if } n_{ij} = 0, \\ 0, & \text{if } n_{ij} \geq 1. \end{cases}$$

2. Generate $\omega_1, \dots, \omega_J$ independently with:

$$\omega_j \mid y_{1j} \dots y_{Ij} \sim \text{Beta} \left(1 + \sum_{i=1}^I y_{ij}, 1 + \sum_{i=1}^I (1 - y_{ij}) \right).$$

3. Run Algorithm S.2 with all (n_{ij}, E_{ij}) such that $y_{ij} = 0$.
-

subsequently renormalized to ensure $\sum_{h=1}^K \eta_{hj} = 1$. The local signal strengths λ_{ij}^l are then initialized for each i using the cluster center (atom) corresponding to the k -means cluster containing point i if $z_{ij} = 1$, or by random sampling from $\theta_{1j}, \dots, \theta_{Kj}$ with probabilities $\eta_{1j}, \dots, \eta_{Kj}$. Finally, the concentration hyperparameter α_j is initialized by random sampling from a Gamma(shape = 1, rate = 2) distribution.

The parameters for the global DP prior are analogously initialized, but using the aggregated observed and expected counts $\{\tilde{n}_i = \sum_{j=1}^{J-1} n_{ij}(1 - z_{ij}), \tilde{E}_i = \sum_{j=1}^{J-1} E_{ij}(1 - z_{ij})\}$ as the data with all AEs i such that $\sum_{j=1}^{J-1} (1 - z_{ij}) > 0$.

Finally, the reference drug J shrinkage hyperparameter τ is initialized at 1, while the zero-inflation parameters ω_j (if included in the model) are initialized each at 0.01.

S.3.3 Optimization method in pFDR calculation

A sequence of threshold values for k , ranging from 1.1 to 3 in small increments, is established. For our computations we specified this grid to be $\{1.1, 1.11, 1.12, 1.13, 1.14, 1.16, 1.17, 1.18, 1.19, 1.2, 1.25, 1.28, 1.31, 1.33, 1.36, 1.39, 1.42, 1.44, 1.47, 1.5, 1.6, 1.76, 1.91, 2.07, 2.22, 2.38, 2.53, 2.69, 2.84, 3\}$. Similarly, a set of distinct small quantile levels for p is chosen ($\{0.01, 0.015, 0.02, 0.025, 0.03, 0.035, 0.04, 0.045, 0.05, 0.055, 0.06, 0.065, 0.07, 0.075, 0.08, 0.085, 0.09, 0.095, 0.1\}$ in our computations). These define a range of possible combinations (p, k) to be considered.

For every quantile level in the p -grid, we obtain a matrix of test statistics $T_{ij}(p)$ based on the p -th posterior quantiles for λ_{ij} computed from their MCMC draws. Subsequently, we compute $\text{FDR}(p, k)$ and $\text{FNR}(p, k)$ estimates using the formulas presented in the main text (Section 3.4) for all possible p and k defined by the grid. From the set of all (p, k) pairs, we then retain only those pairs with computed $\text{FDR} \leq \alpha$ for a preset threshold α ($= 0.05$ in our analyses). Finally, among the retained (p, k) , we identify the pair that minimizes FNR. If multiple (p, k) yield the same minimum FNR, we select the pair with the smallest p and the largest k .

S.3.4 JAGS code for DP Hu et al. model

```

1   # Likelihood
2   for (i in 1:I) {
3     for (j in 1:J) {
4       n[i, j] ~ dpois(E[i, j] * lambda[i, j])
5     }
6   }
7
8   # Prior
9   for (j in 1:J) {
10    alpha[j] ~ dunif(0.2, 10)
11    a[j] ~ dunif(0, 1)
12
13    v[j, 1] ~ dbeta(1, alpha[j]); T(0.00001,0.99999) # to ensure in (0, 1)
14    w[j, 1] <- v[j, 1]
15
16    for (h in 2:K) {
17      v[j, h] ~ dbeta(1, alpha[j]); T(0.00001,0.99999) # to ensure in (0, 1)
18      w[j, h] <- v[j, h] * prod( (1 - c(v[j, 1:(h-1)])) )
19    }
20
21    for (h in 1:K) {
22      theta[j, h] ~ dgamma(a[j], a[j]); T(0.000001, ) # to ensure > 0
23    }
24
25    for (i in 1:I) {
26      ind[i, j] ~ dcat(c(w[j,]))
27      lambda[i, j] <- theta[j, ind[i, j]]
28    }
29  }

```

Listing 1: JAGS exmpale

S.3.5 Example statin dataset

We present the reference SRS contingency table for statin drug in Table S.1. It is used for data generation in Section 4 and data analysis in Section 5.

Table S.1: The SRS contingency table summarized from the FDA FEARS database (Q3 2014-Q4 2020) which catalogs a total of 63,976,610 reported cases.

Adverse Event	Atorvastatin	Fluvastatin	Lovastatin	Pravastatin	Rosuvastatin	Simvastatin	Other
Acute Kidney Injury	1353	42	7	154	689	823	355651
Anuria	71	0	0	2	43	62	10403
Blood Calcium Decreased	14	2	0	0	110	17	15918
Blood Creatine Phosphokinase Abnormal	34	0	0	0	8	11	261
Blood Creatine Phosphokinase Increased	1175	125	32	200	562	768	23805
Blood Creatine Phosphokinase Mm Increased	2	0	0	0	9	0	14
Blood Creatinine Abnormal	27	0	0	0	5	3	3385
Blood Creatinine Increased	227	10	0	17	210	97	74742
Chromaturia	340	10	6	33	174	114	19294
Chronic Kidney Disease	152	16	2	19	177	37	339179
Compartment Syndrome	53	0	0	1	12	12	2644
Creatinine Renal Clearance Decreased	6	0	0	2	124	6	7768
Diaphragm Muscle Weakness	14	0	0	0	8	1	94
Electromyogram Abnormal	2	0	0	2	0	0	132
End Stage Renal Disease	30	0	0	0	19	6	97553
Glomerular Filtration Rate Abnormal	8	0	0	0	1	0	1069
Glomerular Filtration Rate Decreased	59	1	0	8	39	29	13190
Hypercreatininaemia	0	0	0	0	8	0	648
Hypocalcaemia	36	0	0	16	8	18	23102
Muscle Disorder	291	2	7	21	191	87	7329
Muscle Enzyme Increased	48	1	0	0	13	9	410
Muscle Fatigue	85	0	2	16	30	39	4257
Muscle Haemorrhage	24	0	0	5	13	4	3806
Muscle Necrosis	68	2	0	1	10	20	662
Muscle Rupture	181	25	0	61	36	120	3219
Muscular Weakness	1857	45	31	152	808	859	111003
Musculoskeletal Discomfort	137	18	15	25	187	93	19931
Musculoskeletal Disorder	56	3	0	9	65	73	25881
Musculoskeletal Pain	420	3	2	38	324	228	82576
Myalgia	5362	341	151	939	2757	3216	143819
Myasthenic Syndrome	1	0	9	0	3	6	643
Myoglobin Blood Increased	71	4	0	4	16	39	1003
Myoglobin Blood Present	2	0	0	0	0	0	8
Myoglobin Urine Present	0	0	0	0	1	2	70
Myoglobinaemia	15	0	0	0	0	0	62
Myoglobinuria	26	4	0	1	1	9	296
Myopathy	849	64	45	145	377	544	6695
Myopathy Toxic	31	0	0	1	2	21	457
Myositis	219	8	10	28	62	141	7482
Necrotising Myositis	279	0	0	2	10	52	278
Oliguria	52	0	0	4	24	37	7590
Renal Failure	534	26	11	69	225	195	250710
Renal Impairment	390	52	11	37	161	169	103343
Renal Tubular Necrosis	40	0	0	12	10	24	12762
Rhabdomyolysis	2041	52	44	163	936	1376	31707
Tendon Discomfort	9	0	0	3	22	10	794
Other Pt	180699	4886	2845	20296	113960	76068	61724222

S.4 ADDITIONAL SIMULATION RESULTS

We present detailed values of the simulation to compare among our drug (column)-based models (Poisson/ZIP), DP Hu et al., and posterior quantile optimized DP Hu et al. method. Four evaluation metrics (FDR, sensitivity, average type I error, and F-score) are evaluated as well as the main text with same simulation settings in Table 1. Frequentist and Bayesian MSE are compared to further evaluate the loss of the estimation.

S.4.1 Simulation results for DP-based models

We present the four evaluation metrics in Tables S.2, S.3, S.4, and S.5 to provide a clearer numerical comparison beyond Figure 3. Additionally, we further explored the effect of posterior quantile optimization on the DP Hu et al. in the process of FDR control and minimizing FNR. This allows for a more comprehensive understand the strategy of optimizing the posterior quantile of the test statistic and deterministic threshold simultaneously.

We found that in the DP Hu et al. method, simultaneously optimizing the posterior quantile results in only a slight increase in FDR, which remains well-controlled within a very small level (around 0.01). In return, this optimization leads to an improvement in sensitivity, benefiting all cases. When comparing across all DP-based models, the sensitivity gain improvement brought by incorporating the local-global structure is more significant than from this optimization.

Table S.2: Simulation of FDR for DP-based models

Case	λ	DP Poisson local-global	DP ZIP local-global	DP Hu et al.	DP Hu et al. posterior quantile optim
Case 1a Weak correlation No ZI	1.1	0.0035	0.0022	0.0050	0.0102
	1.2	0.0072	0.0063	0.0056	0.0171
	1.3	0.0081	0.0088	0.0053	0.0172
	1.4	0.0074	0.0077	0.0061	0.0168
	1.5	0.0081	0.0079	0.0059	0.0149
	1.7	0.0057	0.0057	0.0050	0.0133
	1.9	0.0049	0.0047	0.0039	0.0108
	2.0	0.0053	0.0056	0.0046	0.0103
	2.5	0.0045	0.0046	0.0043	0.0106
	3.0	0.0031	0.0029	0.0034	0.0086
Case 1b Weak correlation ZI	1.1	0.0010	0.0017	0.0060	0.0197
	1.2	0.0044	0.0034	0.0096	0.0214
	1.3	0.0067	0.0070	0.0070	0.0156
	1.4	0.0086	0.0085	0.0051	0.0157
	1.5	0.0089	0.0092	0.0059	0.0138
	1.7	0.0067	0.0065	0.0056	0.0136
	1.9	0.0058	0.0057	0.0048	0.0117
	2.0	0.0049	0.0050	0.0045	0.0118
	2.5	0.0032	0.0034	0.0032	0.0089
	3.0	0.0036	0.0037	0.0042	0.0095
Case 2a Moderate correlation No ZI	1.1	0.0000	0.0010	0.0065	0.0193
	1.2	0.0107	0.0128	0.0063	0.0150
	1.3	0.0114	0.0132	0.0069	0.0160
	1.4	0.0120	0.0134	0.0060	0.0146
	1.5	0.0095	0.0098	0.0069	0.0157
	1.7	0.0072	0.0079	0.0059	0.0145
	1.9	0.0052	0.0056	0.0058	0.0128
	2.0	0.0042	0.0045	0.0048	0.0125
	2.5	0.0035	0.0035	0.0041	0.0102
	3.0	0.0033	0.0032	0.0032	0.0093
Case 2b Moderate correlation ZI	1.1	0.0000	0.0000	0.0055	0.0122
	1.2	0.0093	0.0106	0.0065	0.0186
	1.3	0.0117	0.0130	0.0069	0.0168
	1.4	0.0102	0.0114	0.0061	0.0153
	1.5	0.0066	0.0076	0.0054	0.0149
	1.7	0.0053	0.0057	0.0058	0.0134
	1.9	0.0039	0.0040	0.0059	0.0126
	2.0	0.0047	0.0050	0.0045	0.0110
	2.5	0.0039	0.0037	0.0042	0.0103
	3.0	0.0030	0.0032	0.0041	0.0094
Case 3a Strong correlation No ZI	1.1	0.0000	0.0000	0.0073	0.0133
	1.2	0.0084	0.0114	0.0074	0.0183
	1.3	0.0073	0.0084	0.0080	0.0184
	1.4	0.0086	0.0096	0.0069	0.0145
	1.5	0.0061	0.0069	0.0067	0.0150
	1.7	0.0045	0.0050	0.0066	0.0136
	1.9	0.0045	0.0050	0.0051	0.0129
	2.0	0.0039	0.0042	0.0049	0.0118
	2.5	0.0033	0.0035	0.0037	0.0096
	3.0	0.0030	0.0029	0.0031	0.0085
Case 3b Strong correlation ZI	1.1	0.0000	0.0000	0.0040	0.0171
	1.2	0.0106	0.0120	0.0084	0.0162
	1.3	0.0077	0.0090	0.0063	0.0161
	1.4	0.0078	0.0083	0.0061	0.0153
	1.5	0.0068	0.0073	0.0051	0.0125
	1.7	0.0044	0.0049	0.0049	0.0119
	1.9	0.0030	0.0032	0.0050	0.0112
	2.0	0.0035	0.0038	0.0052	0.0113
	2.5	0.0033	0.0034	0.0040	0.0092
	3.0	0.0036	0.0037	0.0039	0.0094

Table S.3: Simulation of sensitivity for DP-based models

Case	λ	DP Poisson local-global	DP ZIP local-global	DP Hu et al.	DP Hu et al. posterior quantile optm
Case 1a Weak correlation No ZI	1.1	0.0016	0.0014	0.0009	0.0021
	1.2	0.0427	0.0422	0.0346	0.0435
	1.3	0.1227	0.1243	0.0899	0.1041
	1.4	0.1923	0.1942	0.1432	0.1606
	1.5	0.2444	0.2472	0.1915	0.2115
	1.7	0.3153	0.3180	0.2685	0.2897
	1.9	0.3692	0.3707	0.3258	0.3475
	2.0	0.3926	0.3957	0.3495	0.3720
	2.5	0.4706	0.4729	0.4346	0.4554
3.0	0.5251	0.5273	0.4920	0.5128	
Case 1b Weak correlation ZI	1.1	0.0012	0.0012	0.0011	0.0022
	1.2	0.0406	0.0399	0.0331	0.0416
	1.3	0.1216	0.1232	0.0848	0.1006
	1.4	0.1948	0.1968	0.1401	0.1581
	1.5	0.2426	0.2451	0.1888	0.2102
	1.7	0.3182	0.3196	0.2675	0.2898
	1.9	0.3709	0.3733	0.3261	0.3457
	2.0	0.3921	0.3939	0.3467	0.3678
	2.5	0.4717	0.4742	0.4327	0.4564
3.0	0.5227	0.5253	0.4910	0.5124	
Case 2a Moderate correlation No ZI	1.1	0.0061	0.0060	0.0012	0.0026
	1.2	0.2096	0.2170	0.0526	0.0674
	1.3	0.3304	0.3377	0.1334	0.1530
	1.4	0.3991	0.4036	0.1998	0.2210
	1.5	0.4489	0.4537	0.2499	0.2751
	1.7	0.5172	0.5197	0.3359	0.3637
	1.9	0.5663	0.5681	0.4043	0.4323
	2.0	0.5837	0.5847	0.4310	0.4589
	2.5	0.6396	0.6411	0.5363	0.5608
3.0	0.6734	0.6746	0.5984	0.6214	
Case 2b Moderate correlation ZI	1.1	0.0067	0.0072	0.0011	0.0025
	1.2	0.2067	0.2133	0.0523	0.0659
	1.3	0.3309	0.3367	0.1348	0.1535
	1.4	0.3968	0.4021	0.1973	0.2186
	1.5	0.4438	0.4477	0.2475	0.2723
	1.7	0.5138	0.5157	0.3340	0.3599
	1.9	0.5601	0.5620	0.4000	0.4274
	2.0	0.5772	0.5790	0.4297	0.4570
	2.5	0.6329	0.6339	0.5313	0.5561
3.0	0.6696	0.6708	0.5967	0.6205	
Case 3a Strong correlation No ZI	1.1	0.0065	0.0076	0.0009	0.0020
	1.2	0.2680	0.2784	0.0329	0.0455
	1.3	0.4595	0.4682	0.1088	0.1313
	1.4	0.5675	0.5746	0.1807	0.2100
	1.5	0.6272	0.6330	0.2480	0.2791
	1.7	0.7015	0.7049	0.3546	0.3868
	1.9	0.7460	0.7482	0.4300	0.4612
	2.0	0.7629	0.7644	0.4608	0.4940
	2.5	0.8096	0.8106	0.5793	0.6094
3.0	0.8330	0.8336	0.6530	0.6799	
Case 3b Strong correlation ZI	1.1	0.0083	0.0094	0.0010	0.0021
	1.2	0.2627	0.2769	0.0338	0.0471
	1.3	0.4588	0.4688	0.1098	0.1326
	1.4	0.5638	0.5717	0.1826	0.2115
	1.5	0.6275	0.6333	0.2492	0.2801
	1.7	0.7044	0.7080	0.3534	0.3848
	1.9	0.7485	0.7507	0.4276	0.4599
	2.0	0.7630	0.7651	0.4574	0.4893
	2.5	0.8100	0.8109	0.5787	0.6097
3.0	0.8341	0.8348	0.6556	0.6825	

Table S.4: Simulation of average type I error for DP-based models

Case	λ	DP Poisson local-global	DP ZIP local-global	DP Hu et al.	DP Hu et al. posterior quantile optim
Case 1a Weak correlation No ZI	1.1	0.0000	0.0000	0.0000	0.0000
	1.2	0.0001	0.0001	0.0001	0.0002
	1.3	0.0002	0.0003	0.0001	0.0003
	1.4	0.0002	0.0002	0.0001	0.0004
	1.5	0.0003	0.0003	0.0002	0.0005
	1.7	0.0002	0.0003	0.0002	0.0005
	1.9	0.0002	0.0002	0.0002	0.0005
	2.0	0.0003	0.0003	0.0002	0.0005
	2.5	0.0003	0.0003	0.0002	0.0006
3.0	0.0002	0.0002	0.0002	0.0006	
Case 1b Weak correlation ZI	1.1	0.0000	0.0000	0.0000	0.0001
	1.2	0.0001	0.0001	0.0001	0.0002
	1.3	0.0002	0.0002	0.0001	0.0002
	1.4	0.0003	0.0003	0.0001	0.0004
	1.5	0.0003	0.0004	0.0002	0.0004
	1.7	0.0003	0.0003	0.0002	0.0005
	1.9	0.0003	0.0003	0.0002	0.0005
	2.0	0.0002	0.0002	0.0002	0.0006
	2.5	0.0002	0.0002	0.0002	0.0005
3.0	0.0003	0.0003	0.0003	0.0006	
Case 2a Moderate correlation No ZI	1.1	0.0000	0.0000	0.0000	0.0001
	1.2	0.0005	0.0007	0.0001	0.0002
	1.3	0.0006	0.0008	0.0002	0.0004
	1.4	0.0008	0.0009	0.0002	0.0005
	1.5	0.0006	0.0007	0.0002	0.0006
	1.7	0.0005	0.0006	0.0003	0.0007
	1.9	0.0004	0.0004	0.0003	0.0007
	2.0	0.0003	0.0004	0.0003	0.0008
	2.5	0.0003	0.0003	0.0003	0.0007
3.0	0.0003	0.0003	0.0002	0.0007	
Case 2b Moderate correlation ZI	1.1	0.0000	0.0000	0.0000	0.0001
	1.2	0.0005	0.0006	0.0001	0.0002
	1.3	0.0007	0.0007	0.0001	0.0004
	1.4	0.0006	0.0007	0.0002	0.0005
	1.5	0.0004	0.0005	0.0002	0.0006
	1.7	0.0004	0.0004	0.0003	0.0006
	1.9	0.0003	0.0003	0.0003	0.0007
	2.0	0.0004	0.0004	0.0003	0.0007
	2.5	0.0003	0.0003	0.0003	0.0007
3.0	0.0003	0.0003	0.0003	0.0008	
Case 3a Strong correlation No ZI	1.1	0.0000	0.0000	0.0000	0.0001
	1.2	0.0005	0.0007	0.0001	0.0002
	1.3	0.0006	0.0007	0.0001	0.0004
	1.4	0.0009	0.0010	0.0002	0.0005
	1.5	0.0007	0.0007	0.0003	0.0007
	1.7	0.0005	0.0006	0.0004	0.0008
	1.9	0.0005	0.0006	0.0003	0.0009
	2.0	0.0005	0.0005	0.0003	0.0009
	2.5	0.0004	0.0004	0.0003	0.0009
3.0	0.0004	0.0004	0.0003	0.0009	
Case 3b Strong correlation ZI	1.1	0.0000	0.0000	0.0000	0.0001
	1.2	0.0006	0.0007	0.0001	0.0002
	1.3	0.0007	0.0008	0.0001	0.0004
	1.4	0.0008	0.0009	0.0002	0.0005
	1.5	0.0007	0.0008	0.0002	0.0006
	1.7	0.0005	0.0006	0.0003	0.0007
	1.9	0.0004	0.0004	0.0003	0.0008
	2.0	0.0004	0.0005	0.0004	0.0009
	2.5	0.0004	0.0004	0.0004	0.0009
3.0	0.0005	0.0005	0.0004	0.0010	

Table S.5: Simulation of F-score for DP-based models

Case	λ	DP Poisson local-global	DP ZIP local-global	DP Hu et al.	DP Hu et al. posterior quantile optm
Case 1a Weak correlation No ZI	1.1	0.0030	0.0025	0.0018	0.0040
	1.2	0.0783	0.0772	0.0650	0.0810
	1.3	0.2129	0.2152	0.1615	0.1844
	1.4	0.3180	0.3204	0.2466	0.2722
	1.5	0.3887	0.3924	0.3175	0.3444
	1.7	0.4761	0.4791	0.4200	0.4446
	1.9	0.5358	0.5375	0.4883	0.5115
	2.0	0.5602	0.5634	0.5148	0.5380
	2.5	0.6369	0.6390	0.6027	0.6213
Case 1b Weak correlation ZI	3.0	0.6859	0.6879	0.6566	0.6738
	1.1	0.0023	0.0022	0.0022	0.0042
	1.2	0.0748	0.0733	0.0622	0.0774
	1.3	0.2109	0.2130	0.1531	0.1787
	1.4	0.3212	0.3240	0.2415	0.2682
	1.5	0.3863	0.3894	0.3138	0.3429
	1.7	0.4793	0.4808	0.4187	0.4449
	1.9	0.5378	0.5403	0.4886	0.5094
	2.0	0.5602	0.5621	0.5118	0.5333
Case 2a Moderate correlation No ZI	2.5	0.6382	0.6406	0.6011	0.6226
	3.0	0.6837	0.6859	0.6556	0.6731
	1.1	0.0104	0.0102	0.0024	0.0050
	1.2	0.3333	0.3429	0.0973	0.1231
	1.3	0.4894	0.4973	0.2322	0.2616
	1.4	0.5642	0.5684	0.3299	0.3578
	1.5	0.6141	0.6186	0.3966	0.4269
	1.7	0.6775	0.6796	0.4997	0.5287
	1.9	0.7198	0.7212	0.5724	0.5988
Case 2b Moderate correlation ZI	2.0	0.7344	0.7351	0.5992	0.6242
	2.5	0.7777	0.7789	0.6954	0.7141
	3.0	0.8025	0.8034	0.7463	0.7622
	1.1	0.0114	0.0122	0.0021	0.0049
	1.2	0.3292	0.3375	0.0969	0.1204
	1.3	0.4900	0.4964	0.2345	0.2626
	1.4	0.5624	0.5677	0.3265	0.3548
	1.5	0.6101	0.6136	0.3938	0.4237
	1.7	0.6750	0.6766	0.4975	0.5248
Case 3a Strong correlation No ZI	1.9	0.7150	0.7166	0.5681	0.5941
	2.0	0.7289	0.7303	0.5980	0.6226
	2.5	0.7727	0.7735	0.6911	0.7102
	3.0	0.7999	0.8007	0.7447	0.7614
	1.1	0.0114	0.0131	0.0018	0.0039
	1.2	0.4044	0.4167	0.0623	0.0852
	1.3	0.6199	0.6280	0.1940	0.2290
	1.4	0.7176	0.7231	0.3035	0.3437
	1.5	0.7660	0.7701	0.3947	0.4325
Case 3b Strong correlation ZI	1.7	0.8212	0.8234	0.5209	0.5537
	1.9	0.8515	0.8527	0.5988	0.6270
	2.0	0.8629	0.8638	0.6284	0.6571
	2.5	0.8929	0.8934	0.7314	0.7531
	3.0	0.9072	0.9076	0.7881	0.8055
	1.1	0.0145	0.0162	0.0020	0.0040
	1.2	0.3987	0.4159	0.0639	0.0881
	1.3	0.6192	0.6287	0.1955	0.2312
	1.4	0.7147	0.7211	0.3062	0.3455
1.5	0.7658	0.7702	0.3964	0.4342	
1.7	0.8231	0.8255	0.5197	0.5520	
1.9	0.8537	0.8551	0.5966	0.6261	
2.0	0.8633	0.8645	0.6251	0.6529	
2.5	0.8931	0.8936	0.7308	0.7536	
3.0	0.9076	0.9080	0.7897	0.8071	